Accepted to ApJ
Preprint typeset using LaTeX style emulateapj v. 6/22/04

arXiv:astro-ph/0505485v1 24 May 2005

AN INVESTIGATION OF DIFFUSE INTERSTELLAR GAS TOWARD A LARGE, LOW EXTINCTION WINDOW INTO THE INNER GALAXY

G. J. Madsen[1] and R. J. Reynolds
Department of Astronomy, University of Wisconsin–Madison, 475 N. Charter Street, Madison, WI 53706

Accepted to ApJ

ABSTRACT

Hα and Hβ spectroscopy with the Wisconsin H-Alpha Mapper (WHAM) reveals a strong concentration of high velocity emission in a $\approx 5^\circ \times 5^\circ$ area centered near $(\ell, b) = (27^\circ, -3^\circ)$, known as the Scutum Cloud. The high velocities imply that we are detecting optical emission from near the plane of the Galaxy out to the tangent point at heliocentric distances of $D_\odot \gtrsim 6$ kpc, assuming the gas participates in circular Galactic rotation. The ratio of the Hα to Hβ emission as a function of velocity suggests that dust along these lines of sight produces a total visual extinction of $A_V \approx 3$ at $D_\odot \sim 6$ kpc. This makes it possible to use optical emission lines to explore the physical conditions of ionized gas in the inner Galaxy. At a Galactocentric distance $R_G \approx 4$ kpc, for example, we find that the H$^+$ has an rms midplane density of ≈ 1 cm^{-3} with a vertical scale height of ≈ 300 pc. We also find evidence for an increase in the flux of Lyman continuum photons and an increase in the ratio of ionized to neutral hydrogen toward the inner Galaxy. We have extended the measurements of $E(B-V)$ in this direction to distances far beyond what has been accessible through stellar photometry and find $E(B-V)/N_{\rm H}$ to be near the local mean of 1.7×10^{-22} cm^2 mag, with evidence for an increase in this ratio at $R_G \approx 4$ kpc. Finally, our observations of [N II] λ6583, [S II] λ6716, and [O III] λ5007 toward the window reveal that in the inner Galaxy the temperature of the gas and the ionization state of oxygen increase with increasing height from the midplane.

Subject headings: Galaxy: general—ISM: clouds—dust,extinction—ISM:kinematics and dynamics—ISM:structure

1. INTRODUCTION

A thorough understanding of interstellar matter and processes in the Galaxy requires a full exploration of all phases of the interstellar medium (ISM) in a variety of environments, ranging from the tenuous halo to the energetic nucleus. Diffuse, warm ionized gas is one of the major phases of the ISM of our Galaxy (see reviews by Kulkarni & Heiles 1987; Reynolds 1991a; Mathis 2000; Ferrière 2001). In the solar neighborhood, the warm ionized medium (WIM) consists of regions of warm (10^4 K), low-density (10^{-1} cm^{-3}), nearly fully ionized hydrogen with a scale height of 1 kpc, and appears to be present in every direction in the sky (e.g., Reynolds 1991b; Nordgren et al. 1992; Taylor & Cordes 1993; Haffner et al. 2003). However, the origin and physical conditions within the WIM remain poorly understood. Recent observational studies of the WIM in the solar neighborhood and in the Perseus spiral arm of the Galaxy highlight some of the problems, including how Lyman continuum photons are able to penetrate the seemingly ubiquitous H I to ionize the large-scale WIM, and the inability of photoionization models to explain some of the optical line ratios (e.g., Haffner et al. 1999; Domgorgen & Mathis 1994; Hoopes & Walterbos 2003). Furthermore, the temperature and ionization conditions of diffuse ionized gas in the *inner* Galaxy are likely to differ significantly from the local conditions, given its higher star-formation rate, larger pressure, and stronger UV flux (Heiles et al. 1996a,b; Roshi & Anantharamaiah 2001). The presence of the inner Galactic molecular ring (Dame et al. 2001), for example, suggests that significant star formation is occurring interior to the solar circle.

Investigations of ionized gas through optical emission lines toward the inner Galaxy, especially those regions close to the midplane where the ionizing stars are located, were thought to be prohibitive because interstellar dust severely obscures most of the optical light. As a result, studies of optical and ultraviolet emission sources near the plane are largely constrained to the nearest few kiloparsecs. A potential alternative to optical studies of ionized gas in the inner Galaxy is provided through radio recombination lines (RRLs), free-free emission, and infrared emission, which penetrate the interstellar dust. However, the current sensitivity of RRL and free-free surveys limits these studies to only the brightest regions of ionized gas, with emission measures greater than ~ 500 cm^{-6} pc (Heiles et al. 1996b). In addition, diffuse emission from RRLs may need to be corrected for high n-level effects in order to derive accurate physical properties of the gas, which may be difficult to estimate (Afflerbach et al. 1996; Brocklehurst & Seaton 1972; Shaver 1980). Free-free continuum emission contains no kinematic information, making it difficult to determine the variations in the properties of the ionized gas along the line of sight. Techniques for the detection and study of infrared emission lines from diffuse ionized gas are under development and are currently limited to emission from hydrogen (Kutyrev et al. 2003). Optical emission line studies, on the other hand, are sensitive to much lower apparent emission measures, down to $\lesssim 0.02$ cm^{-6} pc (Madsen et al. 2001; Weymann et al. 2001; Gallagher et al. 2003), and often include lines from a variety of ions from which physical properties of the gas may be inferred. They also have the advantage of being relatively strong and providing velocity information. The principal problem with optical lines is their sensitivity to interstellar extinction.

---

[1] Current address: Anglo-Australian Observatory, P.O. Box 296, Epping, NSW 1710, Australia
Electronic address: madsen@aao.gov.au

To overcome this shortcoming, we can take advantage of the highly non-uniform distribution of interstellar dust, which allows us to see further into the plane at some locations compared to others. Baade's Window, for example, is a well known region of relatively low extinction, about 1° in size, centered near $(\ell, b) = (1^\circ, -4^\circ)$ (Baade 1963). With a total $A(V)$ of only ~ 1.5 out to the center of the Galaxy (Stanek 1996), this piece of sky has been the focus of numerous UV, optical, and IR stellar photometric and spectroscopic investigations used to infer the properties of the Galactic bulge (see review by Frogel 1988). While its small Galactic longitude makes Baade's window well suited for studies of the bulge, the lack of a radial velocity spread toward this direction makes emission line studies of the interstellar medium along the line of sight problematic.

Another much larger, and more suitable, window for ISM studies lies in the direction of the so called 'Scutum Star Cloud'. This $\sim 5^\circ$ diameter 'cloud', centered near $(\ell, b) = (27^\circ, -3^\circ)$, is one of the optically brightest regions of the Galaxy. Its unusually high apparent stellar density led early astronomers to believe it was a region with an enhanced concentration of stars. Subsequently, UV, optical, and IR spectrophotometry of these stars have shown that this area has unusually low extinction, with an $A(V) \approx 2$ out to a distance of 2 kpc (Albers 1962; Karaali et al. 1985; Reichen et al. 1990). The presence of moderate and high velocity emission resulting from differential Galactic rotation, and the observational imprint of dust clouds toward this 'cloud', are evident in the recently completed WHAM survey of the northern sky in Hα (WHAM-NSS, Haffner et al. 2003). Figure 1 provides an Hα map from this survey showing the emission at velocities $v_{\rm LSR}$ between $+35$ km s^{-1} and $+65$ km s^{-1} toward the inner Galaxy. The Hα emission is given in units of Rayleighs[2]. In this general direction, these velocities correspond to emission from the Sagittarius spiral arm of the Milky Way, which is at a distance of about 2–3 kpc (Taylor & Cordes 1993). The large dark feature extending from $(\ell, b) = (50^\circ, 0^\circ)$ to $(\ell, b) = (20^\circ, +10^\circ)$ is the Aquila rift, a well-known, nearby dust cloud ($d \approx 250$ pc, Straižys et al. 2003), which is obscuring the emission behind it with $v_{\rm LSR} \gtrsim +25$ km s^{-1}.

The three spectra underneath the emission line map in Figure 1 show more clearly the effect of extinction by dust. The middle spectrum, toward the Scutum cloud, shows not only emission from the local neighborhood (0 km s^{-1}) and the Sagittarius spiral arm ($\approx +50$ km s^{-1}), but the more distant emission from the Scutum spiral arm ($\approx +75$ km s^{-1}) and all the way out to the tangent point velocity ($\approx +100$ km s^{-1}). The lack of detectable emission at some of these velocities in the other two directions is believed to be caused by the inhomogeneous distribution of interstellar dust. Assuming that ionized gas resides in the Sagittarius spiral arms at an $l \approx 40^\circ$, the leftmost spectrum shows only the weak emission from nearby interstellar gas in front of the Aquila rift. The rightmost spectrum is in a direction which crosses both the Sagittarius and Scutum arms, and shows only emission from local sources and the Sagittarius arm, with dust extinguishing the emission at larger distances. The green box in the emission map outlines the low extinction window, which shows emission all the way out to the tangent point velocity. Of course, the Hα data alone are not enough to confirm that this picture of the distribution of dust along these lines of sight is correct, or that we are detecting emission at large heliocentric distances. The combination of the Hα and Hβ spectra that extend out beyond the tangent point velocity can verify that increased extinction is indeed associated with the emission at increasingly positive velocities.

Here, we report on the detection of high velocity Hα and Hβ emission from the warm, diffuse ionized gas toward the inner Galaxy, including directions toward the Scutum Cloud, and we investigate the nature of the diffuse ISM toward this unique window. We describe our spectroscopic observations in §2, with particular emphasis on the importance of removing atmospheric lines that contaminate the spectra. We present these results in §3, confirming the presence of high velocity Hα and Hβ emission and discussing their relative strengths. A method for estimating the extinction toward this window, based on the Hα and Hβ spectra, is discussed in §4. In §5, we correct the Hα emission for this extinction and infer some intrinsic properties of the ionized gas, including its density and scale height. A comparison between the diffuse Hα and H I emission in this window is presented in §6, including estimates of the relative column densities and flux of ionizing photons in the inner Galaxy. We compare our extinction measurements with the standard, empirical relationship between $E(B-V)$ and N_H along these lines of sight in §7. We discuss observations of [N II] λ6583, [S II] λ6716, and [O III] λ5007 toward a small number of directions in the window and infer some basic physical properties of the ionized gas in §8. We summarize our results in §9.

2. OBSERVATIONS

All of the observations were carried out with the Wisconsin H-Alpha Mapper (WHAM) spectrometer. WHAM consists of a 0.6 m siderostat coupled to a 15 cm dual-etalon Fabry-Perot system (Tufte 1997; Haffner et al. 2003) and produces an optical spectrum integrated over its circular, 1° diameter field of view at a spectral resolution of 12 km s^{-1} within a 200 km s^{-1} wide spectral window that can be centered on any wavelength between 4800 and 7400 Å. WHAM was specifically designed to detect very faint optical emission lines from the diffuse interstellar medium. It is located at the Kitt Peak National Observatory in Arizona and is completely remotely operated from Madison, Wisconsin. The WHAM Northern Sky Survey (WHAM-NSS), carried out between 1997 January and 2000 April, has mapped the entire northern sky ($\delta > -30^\circ$) in Hα within $\approx \pm 100$ km s^{-1} of the local standard of rest (Haffner et al. 2003).

One of the many intriguing results from the WHAM-NSS is the significant amount of Hα emission that appears to extend beyond the Survey's positive velocity limit ($v_{\rm LSR} \approx +100$ km s^{-1}) in a region with $33^\circ < l < 20^\circ, -5^\circ < b < 0^\circ$, particularly in the general direction of the Scutum Cloud. This prompted followup Hα observations obtained between 2002 May and 2002 August that extended the original velocity coverage out to $v_{\rm LSR} = +150$ km s^{-1} over an area within $5° < l < 40°, -5° < b < +5°$. Because these velocities suggested that this emission may be arising from the inner Galaxy, we also obtained Hβ observations toward the same area over the same velocity interval. The Hβ data allows us to quantify the total extinction and the variations of extinction with velocity along the line of sight, and to verify that the emission is arising from large heliocentric distances.

---

[2] $1R = 10^6/4\pi$ photons cm^{-2} s^{-1} str^{-1} $= 2.4 \times 10^{-7}$ erg cm^{-2} s^{-1} str^{-1} at Hα

These new observations were taken in the same manner as the original Survey data (Haffner et al. 2003). The observed region was divided into eight observational 'blocks', with each block covering a $\approx 7° \times 7°$ area. Each direction was observed once in Hα and once in Hβ for 30 sec and 60 sec, respectively. Additionally, 13 individually pointed directions, those which showed the strongest evidence of high-velocity Hα emission, were observed with twice the above exposure times to obtain a higher signal-to-noise ratio. These same 13 directions were also observed in the lines of [N II], [S II], and [O III].

All of the spectra were contaminated by several weak atmospheric emission lines that tarnish the interstellar Galactic spectra (Hausen et al. 2002). The identification and removal of these terrestrial lines from the spectra is essential in order to compare accurately the spectral profiles and relative strengths of the components. In particular, the Hα and Hβ spectra are affected by the relatively bright Hα and Hβ geocoronal emission lines, produced by the excitation of neutral hydrogen in the Earth's atmosphere from scattered solar Lyβ and Lyγ photons, respectively. An additional challenge in the data reduction was the difficulty in characterizing the continuum, because both interstellar and terrestrial emissions are present almost everywhere across the 200 km s^{-1} spectral window. For each spectrum, a least-squares fit was performed, which consisted of the the sum of a linear continuum, atmospheric lines, and the Galactic emission. The determination of the best fit parameters for each of these components of the spectrum, and the subsequent removal of the contaminating atmospheric lines and the continuum, is outlined below for the Hα, Hβ, and other emission line data separately. A more detailed discussion of the data reduction procedure of WHAM data can be found in Haffner et al. (2003).

Another source of systematic uncertainty is the shape of the underlying continuum due to stellar Fraunhofer lines that may be present in diffuse starlight. This effect has yet to be studied quantitatively. The large natural width of the strongest stellar lines, as well as the kinematic broadening along a line of sight, reduces the magnitude of this effect. We see no evidence for significant absorption in our spectra, and have not attempted to make a correction for this effect.

Because of our interest in the ratio of the Hα to Hβ emission as a function of velocity, calibrating the intensities of the two sets of data is important. The Hα spectra were calibrated using synoptic observations of a portion of the North America Nebula (NAN), which has an Hα surface brightness of $I_{\rm H\alpha}$= 800 R (Scherb 1981; Haffner et al. 2003). The Hβ spectra were calibrated by separate Hα and Hβ observations of part of the large H II region surrounding Spica (α Vir), a nearby B1 III star. In the absence of extinction, the photon number ratio of $I_{\rm H\alpha}$ to $I_{\rm H\beta}$ from photoionized gas at a temperature of $T = 8000$ K is 3.94, set by the 'Case B' recombination cascade of hydrogen (Osterbrock 1989; Hummer & Storey 1987). We assume that the emission from the Spica H II region suffers no extinction because of its proximity ($d \approx 80$ pc; Perryman et al. 1997), high Galactic latitude $b \approx +50°$, and the low interstellar hydrogen column density, 1.0×10^{19} cm^{-2}, to the exciting star (York & Rogerson 1976). Combining observations of the Spica H II region with NAN, we obtained a $I_{\rm H\alpha}/I_{\rm H\beta}$ photon ratio of 5.1 toward NAN, consistent with observations of extinction toward stars in the nebula (Cambrésy et al. 2002). All of the Hβ spectra were then calibrated assuming an $I_{\rm H\beta}$= 800/5.1 R = 157 R for NAN. In addition, multiple observations of standard calibration directions were observed at different zenith distances to estimate the nightly transmittance of the atmosphere, allowing an airmass correction to be applied to data.

In order to compare accurately the strengths of [N II], [S II], and [O III] with Hα we needed to apply an additional correction for the difference in transmission of the WHAM instrument at the wavelengths of these lines. This was done by using the Hα and Hβ calibration, and assuming that the change in instrumental transmission is linear with wavelength. This correction is largest for the [O III] data (36%), and very small for [S II] and [N II] (3% and < 1%, respectively). The systematic uncertainty in the response of the spectrometer at the different wavelengths was not formally calculated, and may not vary linearly with wavelength. However, this level of this uncertainty is below the precision of the physical conditions inferred by the data and discussed in §8. In addition, changes in the *ratios* of these lines, which reflect trends in the physical conditions, are not significantly affected by this source of uncertainty.

2.1. *Hα Data*

The geocoronal Hα emission line is the primary contaminant of the Hα data, with an intensity of $I_{\rm H\alpha} \approx 5 - 10$ R that varies with the height of the Earth's solar shadow along the line of sight (Nossal et al. 2001). The line has a narrow width of $5 - 7$ km s^{-1} (FWHM), significantly narrower than the 12 km s^{-1} spectral resolution of WHAM, and it is at rest with respect to the geocentric reference frame. The wavelength of this photo-excited transition is slightly different from that of the Hα produced by recombination (Nossal et al. 2001). For these observations, the geocoronal Hα line was significantly brighter than the relatively wide (≈ 25 km s^{-1}) Galactic emission features, facilitating the use of the geocoronal line as a velocity calibration in each spectrum. However, the motion of the Earth with respect to the local standard of rest (LSR), for the directions and times of these observations, placed the geocoronal line at a velocity $v_{\rm LSR}$ between +20 km s^{-1} and +40 km s^{-1}, obscuring the Galactic emission at these velocities. To remove this geocoronal emission from each spectrum, we modeled it as a single, narrow Gaussian. A first estimate of the strength of the line was provided by visual inspection of the spectrum and theoretical models of the geocoronal line intensity (S. Nossal, private communication).

Several fainter atmospheric lines were also present in every spectrum. These lines have been well characterized through observations near the Lockman window, the direction with the faintest Galactic Hα and H I emission in the sky (Lockman et al. 1986; Hausen et al. 2002). These lines are fixed in a geocentric velocity frame, have narrow widths of ≈ 5 km s^{-1}, and typical intensities of $I < 0.2$ R. The intensity of the lines varies proportionally with the airmass of the observation, and their relative strengths are observed to remain fixed. To correct each spectrum for this effect, we followed a procedure similar to that for the WHAM-NSS reduction. We used a single atmospheric line template based on data from Haffner et al. (2003), with one number, a scaling factor, parameterizing the underlying atmospheric line spectrum.

The remaining artifact to be removed from the spectra is the continuum. As mentioned above, some of the spectra have emission that extends almost all the way across the entire 200 km s^{-1} window. As a result, estimating the location of the continuum was difficult, and this significantly contributes to the overall uncertainty of the resulting interstellar emission profiles. We assume that the continuum is linear in shape Haffner et al. (2003), and took advantage of the fact that most of the spectra suffer from relatively high extinction, and do not appear to contain high-velocity Galactic emission from the more distant gas. These spectral regions, which spanned $\gtrsim 50$ km s^{-1}, were used to estimate the zero point and slope of the continuum, and were consistent with the range of values found for the WHAM-NSS data Haffner et al. (2003). To estimate the continuum for the spectra that *do* exhibit high-velocity emission, an average value of the slope and continuum for spectra within the same block, or nearby block observed on the same night, was used. However, the continuum level and slope is set by the atmosphere as well as the amount of starlight within the beam, which varies from one direction to another.

To remove all of these features from the data, we took additional advantage of the fact that each direction had already been observed once before in Hα during the completion of the WHAM-NSS. These survey spectra have been intensity calibrated and corrected for atmospheric and continuum emission in a more systematic and complete manner, providing an excellent reference for the newer data. The Survey data were also taken at a time when the Earth's motion through the LSR placed the geocoronal line at a different velocity in the Galactic spectrum compared to the newer data. We simultaneously fitted a geocoronal line, continuum, atmospheric line template, and wide (FWHM = 25 km s^{-1}) Galactic emission components to each spectrum. The parameters of the fit were first estimated as discussed above. The best fit continuum and atmospheric emission lines were then subtracted, and the resultant pure Galactic spectrum was compared to the corresponding Survey spectrum at the overlapping velocities (-50 km s^{-1} $\lesssim v_{\rm LSR} \lesssim$ $+100$ km s^{-1}). Small adjustments (generally less than 10%) were then made to the strength of the geocoronal line, the scaling factor for the weaker atmospheric lines, and the shape of the continuum to match the shape of the corresponding Survey spectrum. The remaining difference between the newer data and the Survey spectrum, although small (< 10%), form the largest part of the uncertainty in the Hα data. This systematic source of error comes from small changes in the sensitivity and flat-field of the instrument over a period of ~ 4 years between when the Survey data and the newer data were taken.

2.2. *Hβ Data*

The Hβ data were corrected in a similar manner as the Hα. Each spectrum was modeled as the sum of a linear continuum, a narrow geocoronal Hβ line, weak atmospheric lines, and Galactic emission. However, there were no pre-existing, calibrated Hβ data with which to compare these data. As a result, we were unable to remove the atmospheric contaminants and continuum with same accuracy as the Hα data.

The geocoronal Hβ line is about 10 times fainter than the geocoronal Hα line (Mierkiewicz 2002). With $I_{\rm H\beta} \approx 0.5 - 1.0$ R, it is about as strong as the Galactic Hβ emission components, making its precise position more difficult to determine and thus complicating the removal of the line. A first estimate of the strength and position of the geocoronal Hβ line was made by a least-squares free fit to the spectra. A template of the weaker atmospheric lines was constructed from Hβ observations near the Lockman window, as was done for the Hα data. A single scaling factor was then used to characterize the strength and position of these atmospheric lines in the spectra. Identifying the continuum proved to be the most uncertain aspect of the Hβ data reduction. Lacking any pre-existing Hβ observations, we adopted three values of the continuum that corresponded to a) the best fit to each spectrum and b) upper and lower limits as suggested by the data itself. The best fit was one that minimized χ^2, and the upper and lower limits placed the data points in the flat portions of the spectra entirely below and above the continuum, respectively. This conservative estimate for the continuum uncertainty was incorporated into the overall error estimates, and represents the largest uncertainty in the results.

A model fit to each spectrum was then used to remove the continuum and atmospheric emission lines, as was done for the Hα data. Initial estimates of the parameters of the fit were further constrained by examining the ratio of the Hα to Hβ spectra. If the gas is photoionized, then this ratio should remain constant or increase with velocity or path length, corresponding to a constant or increasing amount of dust along the line of sight. Small changes (≈ 10%) were made to the strength of the geocoronal and atmospheric lines to ensure that the ratio did not decrease, within the uncertainties, over small velocity intervals that corresponded to the position and widths of the atmospheric lines. The small changes were within the generally observed fluctuations in atmospheric line intensity over the timescale of the observations.

2.3. *[N II], [S II], and [O III] Data*

Thirteen sightlines were observed in the additional lines of [N II] λ6583, [S II] λ6716, and [O III] λ5007. These sightlines were chosen based on a preliminary examination of the Hα data that showed the strongest evidence for bright Hα emission at high velocity. The relative strengths of these lines with respect to Hα can be used to estimate the physical conditions of the emitting gas, and to search for potential changes in physical conditions with position in the Galaxy. The quality of these data are not as high as the Hα and Hβ data. However, they allow us to search for important trends in the line ratios and demonstrate the feasibility of a future, more extensive observational campaign to explore physical conditions in the inner Galaxy through nebular emission line diagnostic techniques.

The [N II] and [S II] spectra were reduced in a similar manner as the Hα and Hβ. They were all taken on one night, with each sightline observed once for 180 sec. Each observation covered a velocity interval between -50 $\mathrm{km\,s^{-1}}$ and +150 $\mathrm{km\,s^{-1}}$ LSR. To remove the atmospheric lines from these spectra, a template was used as discussed in §2.1. Emission was present across almost the entire spectrum, and therefore the location of the baseline was difficult to determine. The strength of the Galactic emission was always significantly stronger than the $\lesssim 0.1$ R atmospheric lines; therefore, while estimating the strength of the atmospheric lines was difficult, the error resulting from this uncertainty was small. To determine these parameters, a least-squares fit to the spectra was performed, where the strength of the template and location of the baseline were changed to minimize the χ^2 of the fit. The baseline and template was then subtracted from the spectra. Since the atmospheric lines were much fainter than the Galactic emission, the resulting interstellar emission line profiles are not very sensitive to the particular choice of template strength.

The [O III] data were taken at two different tunes (i.e., two different positions for the center of the spectrometer's 200 $\mathrm{km\,s^{-1}}$ passband) to extend the velocity coverage beyond 200 $\mathrm{km\,s^{-1}}$ and to help in characterizing the baseline. Each direction was observed twice at each tune for 120 sec at a time. The spectra for each sightline at a given tune were averaged together, with the spectra at the different tunes stitched together. The velocity calibration was determined using a semi-empirical prediction based on the pressures of the two etalons. An attempt was made to remove the atmospheric lines based on a template. However, for several spectra the Galactic emission intensity was only comparable to or less than the atmospheric lines, so that small variations in the unknown strength of the atmospheric lines yielded very large uncertainties in the Galactic emission. Therefore, for the [O III] spectra, we adopted an ON-OFF technique, whereby we subtracted one of the [O III] spectra from the rest of the spectra. The OFF spectrum that was subtracted from the other spectra was toward (28°, -2.6°). This direction is close to the Galactic plane where the Hα and Hβ data suggested the $A(V)$ is high, and therefore the Galactic [O III] emission is likely very weak, particularly from the Sagittarius and Scutum arms at $v_{\mathrm{LSR}} \gtrsim 50$ $\mathrm{km\,s^{-1}}$. Since this spectrum was taken close to the other spectra in space and time, the atmospheric lines were accurately removed by this subtraction. This technique underestimates the Galactic [O III] emission, particularly near the LSR, since there may be some Galactic emission toward the OFF direction.

3. DIFFUSE, OPTICAL EMISSION FROM THE INNER GALAXY

The spatial distribution of the highest velocity Hα and Hβ emission is shown in Figure 2. These velocity channel maps cover a smaller area than shown in Figure 1 and highlight the region surrounding the low extinction window. Both of the maps display emission integrated over the velocity range of $+85\ \mathrm{km\,s^{-1}} < v_{\mathrm{LSR}} < +115\ \mathrm{km\,s^{-1}}$, revealing a bright region centered near $(\ell, b) = (27°, -3°)$. The color scaling in Figure 2 has been histogram equalized to enhance the contrast of the features in the map. The morphology of the Hα and Hβ maps are very similar, with a faint halo of emission extending to the south of the brightest knot, and a patchy filament of emission near $l = 33°$. The spectra toward this bright region, at longitudes $l \gtrsim 22°$, reveal distinct emission components centered near $v_{\mathrm{LSR}} \approx +80\ \mathrm{km\,s^{-1}}$ (see Figure 3). The patchy spots of high velocity emission at lower longitudes ($15° < l < 20°$), closer to the Galactic center, are from the wings of much stronger emission centered at lower velocities. At these high velocities, the Hβ emission relative to the Hα emission is about 2.5 times fainter than that predicted for ionized gas with no extinction (Osterbrock 1989; Hummer & Storey 1987), indicating a higher extinction for this gas compared to gas at lower velocities. (see §4 below).

A combination of spatial and spectral information about this high velocity emission is shown in Figure 3. Fifty one directions were selected as having significant emission beyond $v_{\mathrm{LSR}} = +85$ $\mathrm{km\,s^{-1}}$, based on a visual inspection of Figure 2. The Hα and Hβ spectra toward each of these 51 directions is shown, with their position within this figure given by their Galactic coordinates. The horizontal axis of each spectrum is the radial velocity v_{LSR}, spanning a range of $-50\ \mathrm{km\,s^{-1}} < v_{\mathrm{LSR}} < +150\ \mathrm{km\,s^{-1}}$ for each spectrum. The vertical axes are in arbitrary units, and determined individually from the intrinsic brightness of the lines. In two cases, no reliable Hβ spectra were available and are omitted from the figure. The Hβ spectra are represented by the weaker, noisier dark lines, and have been multiplied by 3.94, the expected $I_{\mathrm{H}\alpha}/I_{\mathrm{H}\beta}$ photon ratio in the absence of extinction. Most spectra have two strong, discrete emission features, centered near $v_{\mathrm{LSR}} \approx +50\ \mathrm{km\,s^{-1}}$ and $v_{\mathrm{LSR}} \approx +80\ \mathrm{km\,s^{-1}}$. The H$\alpha$ and Hβ spectra decrease in intensity away from the Galactic plane, and the relative strengths of the Hα and Hβ lines also show that there is less extinction farther from the plane and at lower velocities.

A formal multi-component fit was also made to each of the Hα spectra in Figure 3, from which additional information about the nature of the emission and extinction within the window was obtained (see §4 below). Each reduced spectrum was modeled as the sum of multiple Gaussian components, using a χ^2 minimization scheme similar to the data reduction procedure in §2. The fitted velocity of each component was recorded, and a histogram of those velocities appears in Figure 4. On average, five components were required for a good fit to each spectrum. The full-width half-max (FWHM) of each component was fixed at 25 $\mathrm{km\,s^{-1}}$. This is the typical width of an Hα line in the WHAM-NSS, and is a combination of thermal ($\approx 20\ \mathrm{km\,s^{-1}}$ at $T_e = 10^4$ K) and nonthermal ($\approx 15\ \mathrm{km\,s^{-1}}$) broadening (Haffner et al. 2003). The structure of the histogram was not significantly altered when we allowed the widths of the components to be a free parameter, but not fixing the widths did complicate the fitting procedure, especially for faint, overlapping components. The width of the bins in Figure 4 is 12.5 $\mathrm{km\,s^{-1}}$, half of the FWHM of the components and also the approximate spectral resolution of the WHAM instrument.

The histogram in Figure 4 reveals a strong peak near $v_{\rm LSR} = 0\ \ {\rm km\,s^{-1}}$, which is emission from the local solar neighborhood. It is interesting to note that the peak is slightly red-shifted, consistent with the gas being just interior to the solar circle at these longitudes following a flat rotation curve. There is a second peak near $v_{\rm LSR} = +45\ {\rm km\,s^{-1}}$, which can be interpreted as emission from the Sagittarius spiral arm. Beyond $v_{\rm LSR} \approx +50\ {\rm km\,s^{-1}}$, there is a wide range of velocities all the way out to the tangent point velocity ($\approx +110\ {\rm km\,s^{-1}}$). There is marginal evidence for a concentration of velocity peaks near $v_{\rm LSR} = +70\ {\rm km\,s^{-1}}$, the expected kinematic signature of the Scutum spiral arm. The small number of velocity peaks at $v_{\rm LSR} \geq +120\ {\rm km\,s^{-1}}$ beyond the tangent point velocity are associated with very faint ($\lesssim 0.1$ R) emission and were necessary for a good fit to the data. We note, however, these components may not be physical, and could be part of a higher velocity tail of emission from components at lower velocities with widths greater than 25 ${\rm km\,s^{-1}}$. On the other hand, at least some of these highest velocity components do appear to be associated with gas near the tangent point but with a velocity in excess of that associated with circular rotation (e.g., Lockman 2002a).

4. MEASURING EXTINCTION

4.1. *Formalism*

To characterize further the nature of this high-velocity emission region, we combined the Hα and Hβ data to examine the role of dust extinction along each line of sight. An optically thin photoionized gas at a temperature $T_e = 8000$ K has an intrinsic line ratio of $I_{\rm H\alpha}/I_{\rm H\beta} = 3.94$ in photon units (Osterbrock 1989; Hummer & Storey 1987); this ratio is only weakly dependent on temperature ($\propto T^{0.07}$) and density. Hydrogen gas ionized by other processes, such as shocks, will not emit Hα and Hβ photons in the ratio given above. However, strong shocks from rare supernovae and weaker shocks from spiral arms do not provide enough power to sustain the ionization observed in the general WIM (Reynolds 1990), and therefore we will assume that the diffuse gas observed here is photoionized, and that the recombination ratio $I_{\rm H\alpha}/I_{\rm H\beta}$ can be used to infer the extinction.

Consider a line of sight with an optical depth $\tau_{H\alpha}$ at Hα and $\tau_{H\beta}$ at Hβ out to a point source of emission with an intrinsic brightness $I_{\rm H\alpha,int}$ at Hα and $I_{\rm H\beta,int}$ at Hβ. The ratio of the intensities of the two observed lines is

$$\frac{I_{\rm H\alpha}}{I_{\rm H\beta}} = \frac{I_{\rm H\alpha,int}\ e^{-\tau_{H\alpha}}}{I_{\rm H\beta,int}\ e^{-\tau_{H\beta}}} \quad (1)$$

We replace the intrinsic line ratio $I_{\rm H\alpha,int}/I_{\rm H\beta,int}$ with 3.94 from above, to obtain

$$\ln(\frac{I_{\rm H\alpha}/I_{\rm H\beta}}{3.94}) = \tau_{H\beta} - \tau_{H\alpha} \quad (2)$$

$$= \tau_{H\beta}\,(1 - \frac{\tau_{H\alpha}}{\tau_{H\beta}}). \quad (3)$$

The ratio of $\tau_{H\alpha}/\tau_{H\beta}$ depends on the detailed absorption and scattering characteristics of the dust along the line of sight. However, extinction curves measured in the diffuse ISM of the Galaxy suggest that a fairly well defined relationship exists between the ratio of extinction at one wavelength compared to another. Cardelli et al. (1989), for example, have developed semi-analytical fits to observed extinction curves which parameterizes these ratios through a single scaling factor, the total-to-selective extinction ratio $R_V = A(V)/E(B-V)$. For an $R_V = 3.1$, typical of the diffuse ISM, the ratio of the optical depths $\tau_{H\alpha}/\tau_{H\beta} = 0.70$. To convert the optical depth at Hβ to the more standard quantity of extinction in the Johnson V band, we note that the ratio of optical depths $\tau_{H\beta}/\tau_V$ = 1.16. With the above relationships, and converting τ_V into magnitudes of extinction $A(V)$ through the relation $A(V) = 1.086\,\tau_V$, we obtain $A(V)$ as a function of the observed $I_{\rm H\alpha}/I_{\rm H\beta}$ line ratio:

$$A(V) = 3.12\ln(\frac{I_{\rm H\alpha}/I_{\rm H\beta}}{3.94}). \quad (4)$$

Note that observations of $I_{\rm H\alpha}$ and $I_{\rm H\beta}$ are equivalent to the color excess, or the relative extinction, of the emitting gas. Using equation (2) with the definition of color excess, we see that $\ln[(I_{\rm H\alpha}/I_{\rm H\beta})/3.94] = (1/1.086)\ E(H\beta - H\alpha)$. Normalized extinction curves in the Galaxy, which quantify the relationship between $A(\lambda)$ and $1/\lambda$, are linear at optical wavelengths, and the slope of this line in the optical is not very sensitive to R_V (see review by Fitzpatrick 2004). Therefore, since the difference in the inverse wavelengths between Hα and Hβ, is about the same as the difference between the Johnson B and V bands, the color excess $E(H\beta - H\alpha)$ is similar in value to the commonly measured color excess $E(B-V)$. Using the analytic formalism of Cardelli et al. (1989), the ratio of the two color excesses are

$$\frac{E(H\alpha - H\beta)}{E(B-V)} = 0.12R_V + 0.73 \quad (5)$$

Thus $E(H\alpha - H\beta)$ and $E(B-V)$ differ only by 10% for an $R_V = 3.1$, and never depart from each other by more than 30% for all values of R_V in the Galaxy ($2 < R_V < 5$). As a result, observations of $I_{\rm H\alpha}/I_{\rm H\beta}$ can be used to infer the equivalent value of the color excess $E(B-V)$ with an uncertainty of $\approx$ 10%. However, a value of R_V is required in order to quantify the *total* extinction to the emitting source, $A(V)$.

We note that there is growing evidence that R_V may be systematically lower in the inner Galaxy (Popowski 2000; Udalski 2003). Hα, Hβ, and radio observations of planetary nebulae toward the Galactic bulge suggest that R_V may be as low as 2.0 (Walton et al. 1993; Ruffle et al. 2004). However, there is considerable uncertainty in the distances to these PNe, their association with the bulge, and the derived values of R_V. Our discussion of $A(V)$ below assumes a standard $R_V = 3.1$, but we note that this value may decrease with Galactocentric radius.

4.2. *Caveats*

The discussion above holds true in cases where the Hα and Hβ emission comes from a point source and is subsequently removed from the observer's beam through dust absorption and scattering out of the line of sight. Our observations, however, are of *diffuse* emission. In this case, dust can scatter diffuse light originating from another direction back *into* our 1° diameter beam and $I_{\rm H\alpha}/I_{\rm H\beta}$ is a measure of the attenuation rather than extinction.

This scattering effect complicates the conversion between the observed $I_{\mathrm{H}\alpha}/I_{\mathrm{H}\beta}$ line ratio and the standard definition of interstellar extinction. In order to quantify this effect accurately, detailed radiative transfer models are required, which incorporate the (unknown) distribution of dust and emission, as well as poorly-constrained dust scattering properties (e.g., Mathis 1983; Gordon 2004).

However, this effect is expected to be minimal for emission sources that subtend solid angles that are small compared to the typical scattering angle, which is $\sim 50^\circ$ in the optical (Gordon 2004). Consider a patch of emission in the sky at some distance, with diffuse emission isolated to only that patch in the sky. The solid angle subtended by this emission, as viewed from an average dust particle between the observer and the source, is small. For a patch of emission with an angular diameter of a few degrees, at a distance of a few kiloparsecs, almost all of the dust along the line of sight absorbs and scatters the emission as if it were coming from a point source. As a result, the relationship between $A(V)$ and $I_{\mathrm{H}\alpha}/I_{\mathrm{H}\beta}$ in equation (4) is accurate for measurements toward regions in which the Hα and Hβ emission region is limited to a small region of the sky, with the intervening dust distributed along a large heliocentric distance, as is the case with the high velocity emission toward the Scutum cloud. This accuracy diminishes with decreasing distance between the observer and the source, such as for the very extended emission from the local neighborhood near $v_{\mathrm{LSR}} = 0$ km s^{-1}.

There is an additional complication that must be considered in the relation between $I_{\mathrm{H}\alpha}/I_{\mathrm{H}\beta}$ and $A(V)$. In equation (4), $I_{\mathrm{H}\alpha}$ and $I_{\mathrm{H}\beta}$ represent the total emission from a source, obtained by integrating the total number of Hα and Hβ photons emitted from a single interstellar cloud at some distance, from which an $A(V)$ to the cloud may be measured. However, our observations are of emission along an extended line of sight with sources at different velocities (distances). Each line of sight intersects multiple parcels of warm ionized gas, such as spiral arms, and each parcel has a FWHM ≈ 25 km s^{-1}. Isolating which photons are coming from which 'cloud' becomes formidable if the clouds are not sufficiently separated in velocity. Therefore care must be taken in interpreting the value of $A(V)$ at any one velocity point, especially at a velocity between well-defined peaks in the emission line profile or for profiles in which no strong peaks can be identified. In this case, the *average* value of $A(V)$ over a velocity interval corresponding to the expected width of the line is more representative of the actual value of $A(V)$.

4.3. *Verification*

We can verify the relationship between $I_{\mathrm{H}\alpha}/I_{\mathrm{H}\beta}$ and extinction by comparing our estimates of $E(B-V)$ with direct measurements from stellar spectrophotometry in the same region of the Galaxy. Reichen et al. (1990) used a wide-field, balloon-borne UV imager to study a 6° region centered on the Scutum cloud. Using a combination of photometric and spectroscopic distances, they mapped out the changes in $E(B-V)$ with distance toward stars they detected in the UV. They identified a low extinction window within their 6° field, which is coincident with the directions in which we see high-velocity Hα and Hβ emission. The average of nine WHAM Hα and Hβ spectra that lie in this window, as defined by Reichen et al. (1990), is shown in the top panel of Figure 5.

The shaded regions around the Hα and Hβ spectrum in Figure 5 represent the maximum extent of the uncertainty in the data, combining random and systematic uncertainties. Since the uncertainty in the Hα data comes primarily from systematic uncertainty in the calibration, the uncertainty in one spectrum is correlated with the uncertainty in another. Therefore, the uncertainty in the average Hα spectrum shown in Figure 5 was estimated by taking the difference between the average of the upper limits and the average of the lower limits of all of the spectra. The uncertainty in the Hβ spectra, on the other hand, comes primarily from the uncertainty in the location of the continuum. Assuming that the uncertainty in the location of this baseline is uncorrelated from one direction to another, we estimated the overall uncertainty in the average spectrum to be the average uncertainty of the continuum placement divided by the square root of the number of spectra (9) used to construct the Hβ spectrum in Figure 5. This same method is used for of the all of figures in the paper in which average Hα and Hβ spectra appear. It is important to note that the shaded regions do not represent Poisson errors, but rather the maximum allowable values of the data, given the random and systematic uncertainties.

The bottom panel of Figure 5 shows our inferred values of the color excess $E(B-V)$ as a function of velocity, using $R_V = 3.1$. The shaded region around the dark line is the uncertainty in our inferred value of $E(B-V)$, calculated by combining the upper and lower limits of the average Hα and Hβ spectrum. Only those radial velocities with reasonably low values of the uncertainty are shown, which excludes $v_{\mathrm{LSR}} \lesssim 0$ km s^{-1} and $v_{\mathrm{LSR}} \gtrsim +120$ km s^{-1}. The asterisks are from the data for the UV bright stars from Reichen et al. (1990), and have been placed on this diagram using a distance-velocity conversion from the Galactic rotation curve of Clemens (1985) with $R_\odot = 8.5$ kpc. This rotation curve is used throughout the paper. The vertical dashed line indicates the location of the tangent point velocity. Photometric error bars and distance uncertainties for the stellar data are not provided in Reichen et al. (1990), but they are likely to be large for the faint, distant stars at $D \gtrsim 2$ kpc, corresponding to a $v_{\mathrm{LSR}} \gtrsim +40$ km s^{-1}. We note that the scatter in the stellar $E(B-V)$ data is larger than the uncertainty in the velocity-distance relation that may be caused by deviations from non-circular rotation (Lockman 2002b). Therefore, the scatter is likely related to either the patchiness of the extinction within this region or observational uncertainties. We find that our estimates of $E(B-V)$ match those observed by Reichen et al. (1990), within this scatter.

4.4. *Results*

The assumptions that enter into the conversion between $I_{\mathrm{H}\alpha}/I_{\mathrm{H}\beta}$ and extinction appear valid, and we can therefore use with confidence our observations to estimate extinction toward the inner Galaxy, well beyond that provided by stellar measurements (see Fig. 5). Figure 6 illustrates the low extinction in the window toward the Scutum cloud. The three maps are of the average value of $I_{\mathrm{H}\alpha}/I_{\mathrm{H}\beta}$, calculated by integrating the emission over a 25 $\mathrm{km\,s^{-1}}$ interval, centered at the three indicated velocities. These three velocities are near the location of peaks in the emission profiles toward the Scutum cloud, and are associated with the Sagittarius arm, Scutum arm, and the tangent point velocity. Data with insufficient signal-to-noise have been omitted from the figure. The color scaling has been histogram equalized to enhance the contrast in the maps. The top panel, centered at $v_{\rm LSR} = +50$ $\mathrm{km\,s^{-1}}$, shows several regions with relatively low values of $I_{\rm H\alpha}/I_{\rm H\beta}$ located below the plane near $l \approx 17°, 26°,$ and $37°$. The lower two panels, centered at $v_{\rm LSR} = +75$ $\mathrm{km\,s^{-1}}$ and $+100$ $\mathrm{km\,s^{-1}}$, have much fewer data points due to the lack of measureable Hα and Hβ emission beyond this velocity in many directions, at least in part because of significantly increased extinction. The low extinction region near $(\ell, b) = (26°, -3°)$ is apparent, which persists in the bottom panel centered at $v_{\rm LSR} = +100$ $\mathrm{km\,s^{-1}}$.

The maps in Figure 6 can be used to infer the values of $A(V)$ out to different distances, in different locations in the inner Galaxy. However, for directions away from the Scutum cloud, which is near $l = 26°$, the kinematics of the Galaxy displace the centroids of the emission lines, from gas at the same distance, toward different velocities. Some of these velocities are outside the integration range of each panel in Figure 6. In these directions, the ratio $I_{\rm H\alpha}/I_{\rm H\beta}$ may be an average over the *wing* of a line, and the conversion to values of $A(V)$ and its interpretation, based on the maps in Figure 6, become unclear. It is only toward the Scutum Cloud, where emission lines are centered near the velocities in each panel, that $A(V)$ can be reliably inferred from these maps. The highest velocity components toward this window, centered near $v_{\rm LSR}= +100$ $\mathrm{km\,s^{-1}}$, place the emission at a kinematic distance $D_\odot \gtrsim 6$ kpc. From Figure 6, we see the average ratio $I_{\rm H\alpha}/I_{\rm H\beta}$ centered at this high velocity is ≈ 10, which corresponds to an $A(V) \approx 3$ at this distance (see also Fig. 5).

As a further illustration of this low extinction window, sample spectra toward the Scutum Cloud are shown in Figure 7. The top panels show the Hα and Hβ spectra, with the shaded regions representing their respective uncertainties, as in Figure 5. The Hα spectra are the high intensity, smoother profiles, with the axis labeled on the left side of the panel. The Hβ spectra are the weaker, noisier profiles, with the axis labeled to the right of the panel. The next two panels show the average H I and CO emission in these directions, from the surveys of Hartmann & Burton (1997) and Dame et al. (2001), respectively. The angular resolution of the H I and CO surveys are 0.5°, and the spectra in Figure 7 are averages of the HI and CO observations that lie within the larger 1°WHAM beam. The panel below the CO spectrum shows the Hα to Hβ intensity ratio, and the bottom panel shows the inferred values of $A(V)$ at each velocity point from equation 5, with the uncertainties indicated by the shaded regions. Similar to Figure 5, these panels only show Hα/Hβ and $A(V)$ over velocities in which the uncertainties remain relatively low (i.e., data beyond the tangent point velocity and at $v_{\rm LSR} < 0$ $\mathrm{km\,s^{-1}}$ are not plotted). The horizontal axes are the observable quantity $v_{\rm LSR}$ (bottom of panel) as well as the inferred corresponding kinematic distance (top of panel). The vertical dot-dashed line running through all the panels indicates the location of the tangent point velocity. The horizontal dashed line in the Hα/Hβ plots is at 3.94, the expected ratio in the absence of extinction. Note that in all of the spectra, $A(V)$ remains flat or increases with velocity, as expected from the cumulative effects of attenuation with distance. In two cases, $A(V)$ starts near zero, providing additional confidence in both the data reduction procedure and the conversion from $I_{\rm H\alpha}/I_{\rm H\beta}$ to $A(V)$. Note that some directions exhibit a steep rise in $A(V)$, suggesting the presence of a strong concentration of dust at the corresponding distance (see §6).

The measured values of $A(V)$ at each velocity point allows us to correct our observed Hα profiles for extinction. Figure 8 shows two spectra, one of which has been corrected for extinction. The 'observed' spectrum is an average of nine spectra toward the window, and is the same Hα spectrum from Figure 5. Each observed data point was multiplied by a correction factor of $e^{\tau_{H\alpha}}$, where $\tau_{H\alpha}$ was determined from the Hβ data. In order to produce a smooth profile in the corrected spectrum, the average value of $I_{\rm H\alpha}$ and $I_{\rm H\beta}$ over a 25 $\mathrm{km\,s^{-1}}$ interval for each data point was used to compute $\tau_{H\alpha}$. Figure 8 shows the magnitude of the effect of this extinction correction, and shows that, on average, there may be more emission at larger heliocentric distances near the tangent point, compared to the solar neighborhood and intervening spiral arms. Because of the ambiguity in the velocity-distance relationship in the inner Galaxy, some of the emission near the tangent point could be from gas that lies beyond the tangent point. However, this gas is at a larger Galactocentric distance and z-height, where the density, and contribution the corrected emission measure, is likely to be lower. The corrected spectrum maintains its multiple component features, implying enhanced emission from the Sagittarius and Scutum spiral arms and from the tangent point.

5. SCALE HEIGHT AND DENSITY OF IONIZED GAS

Correcting the observed Hα emission for extinction allows us to infer some intrinsic properties of the ionized gas in the inner Galaxy. Since the Hα emission is related to the emission measure of the gas, $EM = \int n_e^2 dl$, we can extract information about the density and the vertical distribution of H$^+$ by examining the change in the measured $I_{\rm H\alpha}$ in both latitude and distance toward the window. Following the formalism of Haffner et al. (1999), we assume that the ionized gas has a vertical distribution about the Galactic plane with the form

$$n_e(z) = n_e^0 \; e^{-|z|/H} \ \mathrm{cm}^{-3} \qquad (6)$$

where n_e^0 is the density in the midplane and H is the scale height. The relationship between the extinction-corrrected Hα intensity and the gas density is

$$2.75 T_4^{0.9} I_{\rm H\alpha} = \int n_e^2 dl, \qquad (7)$$

where T_4 is the electron temperature of the gas in units of 10^4 K, and $I_{\rm H\alpha}$ is measured in Rayleighs. If we use ϕ to denote the line of sight filling fraction of the emitting gas, and assume that the temperature, filling fraction, and path length through an ionized region are not functions of vertical height z, then we can rewrite equation (7) as

$$I_{\rm H\alpha} = \frac{\phi (n_e^0)^2 L}{2.75 T_4^{0.9}} e^{-2|z|/H} = I_{\rm H\alpha}^0 \; e^{-2|z|/H}, \qquad (8)$$

where $I^0_{\mathrm{H}\alpha}$ is the extinction-corrected Hα intensity at the midplane. Finally, we replace z with $D_\odot$ tan|b|, where $D_\odot$ is the heliocentric distance to the emitting gas at a Galactic latitude b to obtain

$$\ln\, I_{\mathrm{H}\alpha} = \ln\, I^0_{\mathrm{H}\alpha} - \frac{2D_\odot}{H}\tan\,|b|. \quad (9)$$

We now have a relationship between two observable quantities, $I_{\mathrm{H}\alpha}$ and b, from which we may infer the root mean square (rms) midplane density $\phi^{1/2}n^0_e$ and scale height H. Additionally, the low extinction window allows us to isolate emission from different distances and estimate the density and scale height as a function of Galactic radius.

Results of these calculations are shown in Figures 9 and 10. Figure 9 shows the observed quantities of (extinction-corrected) $I_{\mathrm{H}\alpha}$ versus b, while Figure 10 illustrates the inferred quantities of $\phi^{1/2}n^0_e$ and H versus z-height. These data are from spectra toward the low extinction window shown in Figure 3 that lie below the Galactic plane. In order to perform a reliable extinction correction, only those spectra whose integrated intensity exceeded our average systematic uncertainty of 0.1 R were considered. The inferred values of $A(V)$ as a function of velocity were converted into an optical depth, $\tau_{H\alpha}$, at each velocity point by taking the average value of $I_{\mathrm{H}\alpha}/I_{\mathrm{H}\beta}$ within a 25 $\mathrm{km\,s^{-1}}$ interval around each point and applying the relationship in equation (4). This averaging was required because of the finite width of the emission lines, and because some averaging is needed to produce smooth profiles at low intensities.

In order to convert the observed quantities shown in Figure 9 to the inferred quantities in Figure 10, the distance to the emitting gas $D_\odot$ and its pathlength L must be known. Each panel in Figure 9 shows the Hα emission integrated over the three velocity intervals, each 25 $\mathrm{km\,s^{-1}}$ wide, that are centered at $v_{\mathrm{LSR}} = +50, +75, \mathrm{and}\ +100\ \mathrm{km\,s^{-1}}$. These intervals encompass the location of the fitted velocity components shown in Figure 4 and represent emission from the Sagittarius arm, Scutum arm, and near the tangent point. The emission within each interval is assumed to occupy a pathlength $L = 1$ kpc along the line of sight, centered at heliocentric distances $D_\odot = 3.0$, 4.5, and 6.0 kpc, respectively. These distances are consistent with the standard spiral arm model of Taylor & Cordes (1993) and the Galactic rotation curve model from Clemens (1985) with $R_\odot = 8.5$ kpc, as shown in Figure 11. Figure 11 also includes the relationship between v_{LSR} and $D_\odot$ for a flat rotation curve, and shows that the kinematic distances we adopt are not very sensitive to the particular rotation curve that is assumed. We see that the assumed path length, $L = 1$ kpc, is the approximate change in kinematic distance over a 25 $\mathrm{km\,s^{-1}}$ interval for all three selected velocity intervals. We note, however, that non-circular rotation as well as random motions associated with spiral arms, expanding shells, and shear motion may be present along these lines of sight. The magnitude of these effects are generally thought to produce distance uncertainties of less than 10%, but may vary by more than this amount for any individual sight line (Lockman 2002b). A definitive conversion between emission at a particular velocity and a specific distance therefore suffers from this uncertainty, and our adopted distances should be understood as estimates. From equation (9) above, we note that the inferred scale height H is directly proportional to the adopted distance $D_\odot$.

In addition, it may be possible that we are detecting emission from ionized gas beyond the tangent point. This extremely distant emission would appear at lower velocities with increasing distance and, if present, would affect the $D_\odot = 6.0$ kpc emission most, where the velocity 'turn-around' occurs (see Figure 11). Since the overall emission decreases with increasing distance from the plane, the emission from beyond the tangent point, if present, would result in an overestimate of the emission at lower latitudes. However, because the emission beyond the tangent point, at a fixed latitude, is farther away from the plane, it is expected to be much fainter than the emission closer to the Sun. We will assume that this effect is negligible for the $D_\odot = 3.0$ and 4.5 kpc emission, and that for the $D_\odot = 6.0$ kpc emission, the inferred midplane density may be overestimated and the scale height may be underestimated.

For each latitude in Figure 9, there are 2-5 sightlines and thus a range of values for the extinction corrected $I_{\mathrm{H}\alpha}$. The small, filled circles in each panel represent individual observations at different longitudes within the low extinction window. The larger, open circles represent the average value of the individual observations at each latitude. Because there is higher extinction closer the plane, the extinction correction systematically steepens the slope of the data points. The filled circles provide a sense of the magnitude of the variation in the data at each latitude, which is of the same order or smaller than the formal uncertainty of individual observations. The solid line in the figure represents a first-order least-squares fit to the open circles. To estimate the uncertainty in the fit, we assigned a 1σ uncertainty to each filled circle equal to the maximum deviation of the filled circles. The dashed lines in the figure show the extent of the $\pm 1\sigma$ uncertainties in the fitted slope ($-2D_\odot/H$) and intercept ($\ln\, I^0_{\mathrm{H}\alpha}$).

Figure 10 shows the values of these best-fit parameters, with their 1σ uncertainties, converted into the rms midplane density $\phi^{1/2}n^0_e$ and scale height H. Here, the vertical axis has been changed to logarithm of the inferred free electron density, using equation (8) and assuming $T_e = 8000$ K and $L = 1$ kpc. The horizontal axis has been replaced with distance from the Galactic plane, using the adopted distances $D_\odot$ from above. The distance to the emission is also expressed with respect to the center of the Galaxy, R_G, using the average longitude of the data, $< l > \approx 26°$. The best fit rms midplane density increases from 0.54 $\mathrm{cm^{-3}}$ at $R_G \sim 6.0$ kpc to 1.1 $\mathrm{cm^{-3}}$ at $R_G \sim 4.1$ kpc. We note that the conversion to the actual space density n_e within the ionized gas suffers from uncertainty in the poorly constrained path length and filling factor, with $n_e \propto (\phi\ L)^{-1/2}$. The value of ϕ is presently unconstrained. Observations in the neighborhood of the Sun of the warm ionized medium, which has a significantly lower rms density (0.05 $\mathrm{cm^{-3}}$) and larger scale height (1 kpc) than the ionized gas found here, show that it has a filling factor of $\phi \approx 0.1 - 0.3$ (Reynolds 1991b; Nordgren et al. 1992; Mitra et al. 2004).

If the product ϕL does not change considerably with distance, then the data in Figure 10 indicate that the electron density increases toward the Galactic center, although the uncertainty is large for the value inferred nearest to the Galactic center. These results also show that the inferred scale height of the gas, which is computed from the fitted slope, increases toward the Galactic center from H $\approx$ 190 pc at $R_G \sim 6.0$ kpc to H $\approx$ 300 pc at $R_G \sim 4.1$ kpc, although there is some overlap in the uncertainties.

Because the densities and scale heights derived above are significantly different from those derived for the WIM near the Sun, we hesitate to formally identify the emission toward this window with the WIM. This emission appears to characterize ionized gas that is intermediate between the low density, large scale height WIM and the so called Extended Low Density (ELD) H II regions, which have densities $n_e \approx 5 - 10$ cm^{-3} and scale height $H \approx 100$ pc and are detected through radio observations (Mezger 1978), and Br-γ recombination (Kutyrev et al. 2003). Future studies that characterize the properties of ionized gas in the inner Galaxy out to much higher latitudes may help to clarify the nature of this emission and its relationship to the WIM.

6. RELATIONSHIP BETWEEN IONIZED AND NEUTRAL GAS

The relationship between H II and H I, two principal states of interstellar gas within the large-scale diffuse ISM, has yet to be established. The H II may be confined to the outer envelopes of H I clouds embedded in a low-density, hot ionized medium (McKee & Ostriker 1977); the H II may be the fully ionized component of a widespread warm neutral medium (Miller & Cox 1993); or the H II may be well mixed with H I in partially ionized clouds (Spitzer & Fitzpatrick 1993).

An examination of the Hα and H I spectra toward the window, samples of which are shown in Figure 7, offer a starting point for such a study. However, these lines of sight are close to the Galactic plane, where much of the gas may be in molecular form, and where the presence of multiple, interacting sources of ionization may be influencing the dynamics and ionization of the gas in a complicated way. Furthermore, the relatively small size of the window (≈ 30 deg^2) compared to the angular resolution of the Hα and H I observations (~ 1 deg^2) limits a morphological comparison of the two phases. Nevertheless, some general spectral correlations seem to hold true in this region and provide some insight in the relationship between the H I and H II.

From an examination of all of the Hα and H I spectra in the direction of the Scutum cloud, we find that in most cases, kinematically distinct emission components from H II appear near the same velocity as the warm (broad) neutral H I components, and that these velocity components correspond to the Sagittarius and Scutum spiral arms. However, there is little or no correlation between the *strengths* of the H II and warm H I emission. This is consistent with the likely ionization mechanism of hydrogen. If the H II is photoionized, then as long as the H I is opaque to Lyman continuum photons ($N_{\rm HI} \gtrsim 10^{18}$ cm^{-2}), the emission measure from Hα is related only to the intensity of the ionizing flux and is thus unrelated to the total column density of H I. Interestingly, there are some directions in which very little high velocity H I emission is present, yet there is substantial Hα emission. An example of this is seen in the inner Galaxy near $v_{\rm LSR} = +100$ km s^{-1} in the three rightmost panels of Figure 7. This comparison would look even more dramatic if the 21 cm spectrum were compared to extinction corrected Hα profiles, as shown in Figure 8. These observations suggest that the ISM is substantially ionized in these regions, with the H I perhaps confined to small, unresolved H I clouds that populate the inner Galaxy (Lockman 2002a).

We can compare the column densities of the ionized and neutral gas. The midplane rms space density of electrons at different distances, over 1 kpc intervals, is estimated in §5 and shown in Figure 10. Multiplying these space densities by 1 kpc yields midplane column densities $N_{H^+} = 1.7\phi^{1/2}$, $2.3\phi^{1/2}$, and $3.3\phi^{1/2} \times 10^{21}$ cm^{-2} at heliocentric distances $D_\odot = 3.0$, 4.5, and 6.0 kpc, respectively. Integrating the average H I spectra at $b = 0°$ between $22° < l < 28°$ from Hartmann & Burton (1997) over the same velocity/distance intervals, yields midplane column densities $N_{HI} = 3.1$, 2.9, and 3.5×10^{21} cm^{-2}. We note that column densities of H^+ are upper limits, because its volume filling fraction ϕ is less than 1. In addition, the column densities of H I may be lower limits, because of potential H I self-absorption features in H I spectra near the Galactic plane (e.g. Gibson et al. 2000). Therefore, the fraction of gas that is ionized, $N_{H^+}/(N_{H^+} + N_{HI})$, at each of these locations in the inner Galaxy are upper limits. If ϕ and 21 cm absorption effects are the same at all distances, then the relative amount of H II increases toward the Galactic center, with values of $N_{H^+}/(N_{H^+} + N_{HI})$ given by $0.35 : 0.44 : 0.49$ at $R_G \sim 6.0$, 4.9, and 4.1 kpc, respectively.

The extinction-corrected values of $I_{\rm H\alpha}$ are a direct measure of the flux of Lyman continuum photons (e.g., Tufte et al. 1998). An H I cloud illuminated on one side by a flux F_{LC} of ionizing photons emits one Hα photon for every 2.05 Lyman continuum photons absorbed, provided the gas is optically thick to the Lyman continuum photons and optically thin at Hα (Osterbrock 1989). For a cloud embedded in a uniform field of Lyman continuum radiation, the intensity of Hα is increased by a factor of 2, because there are two illuminated surfaces in projection. Therefore $I_{\rm H\alpha}$ toward a collection of N_C clouds bathed in a Lyman continuum flux F_{LC} is given by

$$F_{LC} = 2.05 \times 10^6 \, \frac{I_{\rm H\alpha}}{2N_C} \text{ photons cm}^{-2} \text{ s}^{-1} \qquad (10)$$

with $I_{\rm H\alpha}$ measured in Rayleighs. From the fits shown in Figure 9, our observations indicate that the extinction corrected midplane Hα intensity is $I^0_{\rm H\alpha} \approx$ 130, 250, and 490 R at heliocentric distances $D_\odot =$ 3.0, 4.5, and 6.0 kpc, respectively. This corresponds to a one-sided Lyman continuum flux of $F_{LC} = 1.3/N_C$, $2.6/N_C$, and $5.0/N_C \times 10^8$ photons cm^{-2} s^{-1}. If there is the same number of clouds present in each 1 kpc interval over which $I_{\rm H\alpha}$ was measured, then the flux of ionizing radiation increases by a factor of 4 from $R_G \sim 6.0$ kpc to $R_G \sim 4.1$ kpc.

Thus both the Lyman continuum flux and the fractional amount of H$^+$ appear to increase toward the inner Galaxy. This is consistent with many observations that suggest an increase in star formation activity in the Galaxy interior to the solar circle.

7. RELATIONSHIP BETWEEN GAS AND DUST

In addition to the Hα and H I spectra, a relationship appears to exists between features in the molecular CO emission spectra and values of $A(V)$ derived from the optical Hα and Hβ emission. Samples of these data are shown in Figure 7. As discussed in §4, $A(V)$ remains flat or increases with velocity (distance) in all directions, consistent with the cumulative effects of extinction with distance. In some cases, a sharp rise in $A(V)$ is evident, indicative of the presence of a dense concentration of dust. The leftmost panel in Figure 7, near $v_{\rm LSR} = +60$ km s^{-1}, shows an example of this. Not suprisingly, we find strong CO emission at the same velocities as this sharp rise in $A(V)$, confirming the well-known correlation between the presence of molecular gas and interstellar dust. In other cases, such as in the second panel from the left in Figure 7, $A(V)$ rises smoothly in the absence of strong CO emission, suggesting that interstellar dust is more smoothly distributed along the line of sight.

These independent measurements of the extinction, when combined with H I and CO spectra, allow us to quantify the relationship between the dust and gas content toward the window. Bohlin et al. (1978) investigated the relationship between the color excess $E(B-V)$ and the total neutral hydrogen column density, $N_{\rm H} = N_{HI} + 2N_{H_2}$, toward a population of several nearby ($d \lesssim 2$ kpc) hot stars. Their observations traversed sightlines with $E(B-V) < 0.5$, from which they determined a "definitive value" of $N_{\rm H}/E(B-V) = 5.8 \times 10^{21}$ atoms cm^{-2} mag^{-1}. This quantity is cited often and is used to estimate color excesses (and extinction corrections) for objects in which $E(B-V)$ cannot be determined directly.

The lines of sight to the low extinction window contain substantially more dust and gas than those studied in Bohlin et al. (1978). However, the same kind of analysis can be made, and it can be compared with their canonical value. Any cumulative change in this value over a very long distance can also be assessed. Figure 12 summarizes this analysis. The top panel shows the average Hα and Hβ spectra toward five lines of sight toward the Scutum cloud. As with the previous figures, the total uncertainty in the spectra are shown as the shaded regions around the spectra, and the Hβ spectra have been multiplied by 3.94, the ratio of $I_{{\rm H}\alpha}/I_{{\rm H}\beta}$ in the absence of extinction. These five directions were chosen because of their low uncertainty in $A(V)$, presence of high-velocity emission, and low CO emission line strength. This increased the accuracy of our determination of $N_{\rm H}/E(B-V)$, and avoided directions where CO self-absorption may be present (Minter et al. 2001; Jackson et al. 2002). The second and third panels show the average H I and CO spectra within the WHAM beam in these directions, from the surveys of Hartmann & Burton (1997) and Dame et al. (2001), respectively. The straight line at high velocities in the CO spectra indicate a lack of data at those velocities. The fourth panel shows the cumulative column density of H I, along with H I + 2H$_2$, as a function of distance in units of 10^{21} cm^{-2}. This is calculated by integrating the H I and CO spectra from $v_{\rm LSR} \approx -20$ km s^{-1} out to each velocity point, using a CO-to-H$_2$ mass conversion factor of $X = 1.8 \times 10^{20}$ cm^{-2} (K km s^{-1})$^{-1}$ from Dame et al. (2001). We note that while the CO spectra appear quite noisy, there exists a positive signal which significantly contributes to the total neutral hydrogen column density at the higher velocities. The fifth panel shows the inferred values of the color excess $E(B-V)$ along with its uncertainty. The values of $E(B-V)$ are only shown over the velocity interval in which the uncertainties are low. The bottom panel shows the ratio of $E(B-V)/N_{\rm H}$, in units of mag per 10^{21} cm^{-2}, along with a solid horizontal line at the location of the canonical value from Bohlin et al. (1978). Note that this is the inverse of the quantity $N_{\rm H}/E(B-V)$ discussed in Bohlin et al. (1978).

Out to $v_{\rm LSR} \approx +80$ km s^{-1}, our derived value agrees with the value from Bohlin et al. (1978). Beyond this velocity, there is an increase in the amount of extinction per unit hydrogen column density, by about a factor of two. As seen in Figure 12, this is the result of an increase in $E(B-V)$. We note that the potential presence of very faint, broad Hα and Hβ emission in the spectra would have been removed by our continuum subtraction process, particularly at the highest velocities. This effect would result in an underestimate of the Hα emission relative to Hβ, and would increase the derived value of $E(B-V)/N_{\rm H}$ over its already enhanced value. In addition, since we are measuring the *cumulative* extinction and column density, this increase suggests that the local value of this number in the inner Galaxy, at $D_\odot \gtrsim 5$ kpc, is even higher than the observed value of ≈ 0.3 mag per 10^{21} cm^{-2}. If a constant, elevated value is present only over the last third of the distance out to the tangent point, as the figure suggests, than the local value near the tangent point is ≈ 0.6 mag per 10^{21} cm^{-2}, more than 3 times greater than the value near the Sun.

Recent work by Lockman & Condon (2005) have found the opposite trend toward regions with very low reddening. Using high sensitivity H I observations at high Galactic latitude, they find that $E(B-V)/N_{\rm H} \approx 0.1$ mag per 10^{21} cm^{-2}, which is almost half of the canonical value. Their data included sightlines with H I column densities that are ≈ 10 times below those included in Bohlin et al. (1978). When combined with our results, it appears that the amount of reddening per unit hydrogen atom in the Galaxy is not a constant. Another parameter, perhaps related to the total $N_{\rm H}$ and/or Galactic environment, may be important in understanding the relationship between $E(B-V)$ and $N_{\rm H}$.

We note that although our derived values within 4 kpc of the Sun fall near the canonical value, there are several uncertainties in this analysis. Most importantly, Bohlin et al. (1978) were able to directly measure both $E(B-V)$ through stellar photometry as well as $N_{\rm H}$ through UV absorption lines, whereas we have used $I_{{\rm H}\alpha}/I_{{\rm H}\beta}$ as a proxy for the extinction, and the emission lines from H I and CO to estimate the total neutral hydrogen column. To address some of the caveats regarding our estimates of the extinction, particularly with the potential blending of the emission components, we have modeled the average Hα and Hβ spectra as a sum of multiple Gaussian components, and compared the ratio of these individual components to the smooth curve of $E(B-V)$. Each of the five Hα spectra were fitted with five components, with fixed widths of 25 km s^{-1}. The Hβ spectra were fitted by fixing both the width and location of the components, as determined from the fit to the corresponding Hα spectra, since this emission comes from the same atoms. The ratio of each of these components was converted into $E(B-V)$, and these are shown as dark circles in the fifth panel of Figure 12. This method yields ratios that are consistent with the smooth, average curve, showing that the blending of the emission lines is not an important effect. In addition, the relationship between $I_{\mathrm{H}\alpha}/I_{\mathrm{H}\beta}$ and $E(B-V)$ is not very sensitive to potential changes in R_V along these lines of sight toward the inner Galaxy, as discussed in §4.

Our calculation of N_{H} is also subject to some uncertainty. The intensity of CO spectra are near the level of the quoted uncertainty in the CO survey. However, when integrated over all velocities, the integration yields a result several standard deviations away from the noise. The uncertainty in the cumulative CO emission is smallest at the highest velocities. The subsequent conversion from this value to an H_2 column density is not very well constrained. The conversion factor, X, is known to vary in different environments, particularly in regions with non-solar metallicities, as is the case in the inner Galaxy (Wilson 1995; Simpson et al. 2004). The higher metallicity in the inner Galaxy would result in a conversion that overestimates the actual N_{H_2} at the higher velocities, which in turn would further increase our derived value of $E(B-V)/N_{\mathrm{H}}$ over its already enhanced value. However, by selecting directions with low CO emission line strengths, we may have introduced a bias in our results which may not hold true for other sightlines in the inner Galaxy.

If the dust properties in the *ionized* gas are similar to those in the neutral medium, then the increasing fraction of H^+ toward the inner Galaxy (§6) would correspondingly increase $E(B-V)/N_{\mathrm{H}}$. However, the 40% increase derived for $N_{H^+}/(N_{H^+}+N_{HI})$ is far too small to account for a factor of three increase in $E(B-V)/N_{\mathrm{H}}$.

The uncertainty in the beam filling factor of H I and CO emission within the 1° WHAM beam also may bias our results. These measurements were taken with a single dish telescope, and therefore clumping of the emission into small knots can change the interpretation of the data. For example, consider a 'two-phase' medium, in which the column density of dust and neutral gas are bimodally distributed between two values in the beam. For a fixed average column density, this clumpiness results in differentially more light passing through the lower extinction regions, reducing the effective optical depth. Our analysis of $E(B-V)/N_{\mathrm{H}}$ has assumed that the radio emission is smoothly distributed over some path length within the beam. If this is not true, then our derived values of $E(B-V)/N_{\mathrm{H}}$ should be considered lower limits, with this ratio elevated toward higher-density 'clumps' within a 1° beam. The observed variation in the total column density of CO and H I among the five beams vary by a factor less than 2. If a density contrast of a factor of 2 between two 'phases' is present within a beam, then for an average total column density of 4×10^{21} cm^{-2}, the effective $E(B-V)/N_{\mathrm{H}}$ is reduced by 10% at most, for all values of the relative areal filling factor of the two phases. A reduction by 50% is not reached until the density contrast reaches 10, and then only for a limited range in areal filling factors. We conclude that our values of $E(B-V)/N_{\mathrm{H}}$ are not strongly affected by such systematic uncertainties.

8. PHYSICAL CONDITIONS OF THE IONIZED GAS

Observations of the emission lines of [N II], [S II], and [O III] can be used to explore the physical conditions of gas by comparing the strength of these lines to that of Hα. For example, [N II]/Hα traces variations in the electron temperature of warm ionized gas, assuming that the gas is photoionized and that that ionization fraction of N^+/N is not changing (Haffner et al. 1999; Reynolds et al. 1999). The line ratio of [S II]/[N II] is nearly temperature independent and can be used to estimate the ionization fraction of S^+/S, while the ratio [O III]/Hα is a measure of the higher ionization states of the gas. These lines have been used to characterize diffuse warm ionized gas within ≈ 2 kpc of the Sun (e.g., Haffner et al. 1999). Observations of these lines toward the low extinction window provide a new and unique opportunity to examine the potential changes in the physical conditions of the gas toward the inner Galaxy.

Results from some of our observations of these lines are shown in Figure 13. Spectra taken at the same latitude within the window have been averaged over longitude and appear in each of the panels in the figure. The left panels shows the spectra of Hα (*black*), [N II] (*red*), and [S II] (*green*) with increasing $|b|$, where [N II] and [S II] have been multiplied by 2 to facilitate the comparison of the relative line strengths. The right panel shows the spectra of Hβ (*black*) and [O III] (*purple*), where [O III] has been multiplied by a factor of 10 for comparison. The similarity of wavelengths for spectra in each of the two panels greatly reduces the effect of extinction on the relative line strengths.

There are several interesting trends in the data. While the Hα emission becomes weaker at higher $|b|$, both [N II]/Hα and [S II]/Hα increase. At a given latitude, [S II]/[N II] tends to decrease with increasing distance (velocity). This effect is greatest for the $b=-4.3°$ data. There are significant changes in [O III]/Hβ with both latitude and distance. At $b=-1.7°$, there are two velocity components in the [O III] spectrum that correspond to components in the Hβ spectrum, with [O III]/H$\beta \sim 0.05$ for both components. With increasing distances from the plane, [O III]/Hβ associated with gas in the inner Galaxy (near the tangent point) increase by a factor of four or more, from 0.05 at $b=-1.7°$ ($z=-180$ pc) to about 0.2 at $b=-4.3°$ ($z=-450$ pc).

A more quantitative description of these line ratios are shown in Table 1. The spectra have been integrated over four discrete velocity intervals, centered at +25, +50, +75, and +100 $\mathrm{km\,s^{-1}}$, with a width of 25 $\mathrm{km\,s^{-1}}$. The Hα and Hβ data were used to estimate the extinction $A(V)$ as discussed above. The extinction at the wavelengths of the other emission lines was calculated from Cardelli et al. (1989). All of the data in the table have been corrected for extinction, and the line ratios are given in energy units.

We find that [N II]/Hα increases from ~ 0.4 to ~ 0.6 as b decreases from $-1.7°$ to $-4.3°$, at all velocities. This variation could be due to changes in the ionization state of N, the abundance of N, or the temperature. If it is only temperature that is changing, then the data suggest that T_e increases from ~ 7000 K to ~ 8000 K with increasing height above the plane, assuming $\mathrm{N/H} = 7.5\times10^{-5}$ and $\mathrm{N}^+/\mathrm{N} = 0.8$ (Meyer et al. 1997; Sembach et al. 2000).

This increase in temperature in regions of lower Hα emission, or lower density, is consistent with several similar observations throughout the WIM (Haffner et al. 1999). However, the abundance of N, relative to H, changes with distance from the Galactic center (Afflerbach et al. 1997), with N/H greater by about a factor of 1.8 in the inner Galaxy (Simpson et al. 2004). In this case there is an increase in T_e of about $\sim$ 700 K from $b = -1.7^\circ$ to -4.3°, and the overall temperatures are lower by about 1000 K than those quoted above.

The interpretation of [S II]/[N II] also suffers from an uncertainty in the assumptions about the physical state of the gas. However, if variations in [S II]/[N II] are due only to changes in the ionization fraction of S^+/S (i.e., N^+/N is constant), then the data suggest that S^+/S increases from $\sim$ 0.25 to $\sim$ 0.4 with increasing $|b|$ for the nearby gas, and is relatively constant at $\sim$ 0.25 in the inner Galaxy, assuming S/H = 1.86×10^{-5} (Anders & Grevesse 1989).

The [O III] data for the inner Galaxy show a definitive increase in [O III]/Hα with increasing distance from the plane. This increase in the inner Galaxy is much larger than the uncertainty in the line ratios and is in contrast to other observations of the WIM in the solar neighborhood that show [O III]/Hα *decreasing* with distance above the plane (Madsen et al. 2005, in preparation). The line ratios are all less than $\sim$ 0.06, which is consistent with other observations in the diffuse WIM, and is considerably less than what is observed in traditional H II regions. The increase in [O III]/Hα with $|b|$ could be due to several effects, including an increase in temperature or contributions from shock ionization (i.e., increase in the abundance of O^{++}). An increase in T by 1000 K (see above) would increase the [O III]/Hα ratio by about a factor of 2, which is much less than what is observed (Table 1). This suggests that the O^{++}/H^+ ratio also increases with increasing $|z|$ in the inner Galaxy, as has been suggested by observations in other galaxies (e.g., Rand 1997).

9. SUMMARY

We have detected diffuse Hα emission from warm ionized gas toward the inner Galaxy at velocities that place the gas near the tangent point. Observations of the Balmer decrement confirm that we are seeing optical emission a few degrees away from the Galactic plane at heliocentric distances greater than $\approx$ 6 kpc. We have characterized the extinction in this region and identified a $\sim 5^\circ\times5^\circ$ low extinction window centered near $(\ell, b)=$ (27°, -3°) with a total $A(V) \sim 3$ out to the tangent point.

This unique window into the inner Galaxy provides an opportunity to investigate potential changes in the nature of the diffuse interstellar medium in different Galactic environments using optical nebular emission line diagnostic techniques. The Hα and Hβ spectra have emission line profiles that are consistent with emission from the local neighborhood, the Sagittarius spiral arm, the Scutum spiral arm, and beyond. We have used a model for the rotation of the Galaxy to infer a distance to these emission components, and to derive the distribution and density of the gas. The rms midplane density and the scale height increase toward the center of the Galaxy, with $\phi^{1/2}n_e^0 \approx$ 0.54, 0.75, and 1.1 cm^{-3} and $H \approx$ 190, 270, and 300 pc at $R_G \sim$ 6.0, 4.9, and 4.0 kpc, respectively. A comparison between Hα and H I emission in this window suggests that the warm ionized gas may be associated with the surfaces of warm neutral gas clouds. The Hα and H I data also suggest that the flux of Lyman continuum radiation increases by a factor of $\approx$ 3 and the fraction of hydrogen that is ionized increases by a factor of $\sim$ 1.5 from $R_G = 6$ kpc to 4 kpc toward the inner Galaxy. We have combined our extinction measurements with H I and CO data and found that within $\sim$ 6 kpc of the Sun, the amount of extinction per unit neutral hydrogen, $E(B-V)/N_{\rm H}$ is similar to the canonical value of Bohlin et al. (1978). We also found evidence that this ratio increases by a factor of $\approx$ 2-3 at a Galactocentric radius $R_G \lesssim 4$ kpc, and suggest that $E(B-V)/N_{\rm H}$ varies with Galactic environment. Observations of emission from the other ions of [N II], [S II], and [O III] suggest that the temperature and ionization state of the gas in the inner Galaxy increases with increasing distance from the Galactic plane.

Traditional studies of extinction in the Galaxy, through star counts and stellar spectrophotometry, are focused toward directions of the sky containing stars with reliable distances and sufficient brightness, limiting these techniques to distances of about 2 kpc. The method of using the Balmer emission line decrement from diffuse ionized gas, presented here, has the advantage of being able to measure the extinction out to much larger distances, provided there is strong enough emission and/or low enough extinction, as in the case of the Scutum Cloud. This approach is most reliable for patches of diffuse emission at the largest distances, and is best suited for mapping out extinction toward distant, low $A(V)$ windows, complementing the locally derived extinction from stellar data. This technique is also limited to directions in which the relationship between velocity and distance can be reliably determined. Several models for the distribution of $A(V)$ in the Galaxy exist, and employ a variety of observational and theoretical, and semi-empirical methods over a range of optical and infrared wavelengths (Schlegel et al. 1998; Hakkila et al. 1997; Drimmel et al. 2003). A large survey of Hα, Hβ, and perhaps Br-γ near the Galactic plane, using the observational technique described here, will help constrain these models and may lead to a more accurate understanding of the three dimensional structure of gas and dust in the Galaxy.

The origin of this large window is not clear. The total neutral atomic hydrogen column density, as measured through the 21 cm emission line, is not substantially lower in this window compared to regions around it, although H I self-absorption and 21 cm emission from beyond the tangent point must also be considered. Velocity channel maps of H I do not show evidence for a cavity or supershell, as has been found in the Scutum supershell near $(\ell, b)=$ (18°, -4°) (Callaway et al. 2000). Emission from CO is elevated in some regions outside the window, consistent with the well-known correlation between the presence of optically obscuring dust and molecular gas. However, diffuse infrared emission is neither enhanced nor suppressed substantially toward the window, as seen in maps from the IRAS and MSX instruments. There is no enhancement in the X-ray emission maps from ROSAT, although the large columns of H I would absorb most of the soft X-rays from the inner Galaxy. Future spectroscopic investigations toward this area of the Galaxy, including deep spectrophotometry of distant stars, may help to understand the origin of this window as well as the nature of the gas, dust and stars in the inner Galaxy.

10. ACKNOWLEDGEMENTS

We thank the anonymous referee for a thorough review and helpful suggestions which improved the paper. We are grateful to John Mathis for his insightful conversations about the nature of interstellar dust, and to L. Matt Haffner, Steve Tufte, and Kurt Jaehnig for their important roles in the continued success of WHAM. WHAM was built and continues to explore the warm ionized medium through the generous support of the National Science Foundation through grants AST96-19424 and AST02-04973. GJM acknowledges additional support from the Wisconsin Space Grant Consortium.

REFERENCES

Afflerbach, A., Churchwell, E., Acord, J. M., Hofner, P., Kurtz, S., & Depree, C. G. 1996, ApJS, 106, 423
Afflerbach, A., Churchwell, E., & Werner, M. W. 1997, ApJ, 478, 190
Albers, H. 1962, AJ, 67, 24
Anders, E., & Grevesse, N. 1989, Geochim. Cosmochim. Acta, 53, 197
Baade, W. 1963, Evolution of Stars and Galaxies (Cambridge, MA: Harvard University Press), 277
Bohlin, R. C., Savage, B. D., & Drake, J. F. 1978, ApJ, 224, 132
Brocklehurst, M., & Seaton, M. J. 1972, MNRAS, 157, 179
Callaway, M. B., Savage, B. D., Benjamin, R. A., Haffner, L. M., & Tufte, S. L. 2000, ApJ, 532, 943
Cambrésy, L., Beichman, C. A., Jarrett, T. H., & Cutri, R. M. 2002, AJ, 123, 2559
Cardelli, J. A., Clayton, G. C., & Mathis, J. S. 1989, ApJ, 345, 245
Clemens, D. P. 1985, ApJ, 295, 422
Dame, T. M., Hartmann, D., & Thaddeus, P. 2001, ApJ, 547, 792
Domgorgen, H., & Mathis, J. S. 1994, ApJ, 428, 647
Drimmel, R., Cabrera-Lavers, A., & López-Corredoira, M. 2003, A&A, 409, 205
Ferrière, K. M. 2001, Rev. Mod. Phys., 73, 1031
Fitzpatrick, E. L. 2004, in ASP Conf. Ser. : Astrophysics of Dust, in press
Frogel, J. A. 1988, ARA&A, 26, 51
Gallagher, J. S., Madsen, G. J., Reynolds, R. J., Grebel, E. K., & Smecker-Hane, T. A. 2003, ApJ, 588, 326
Gibson, S. J., Taylor, A. R., Higgs, L. A., & Dewdney, P. E. 2000, ApJ, 540, 851
Gordon, K. D. 2004, in ASP Conf. Ser. : Astrophysics of Dust, in press
Haffner, L. M., Reynolds, R. J., & Tufte, S. L. 1999, ApJ, 523, 223
Haffner, L. M., Reynolds, R. J., Tufte, S. L., Madsen, G. J., Jaehnig, K. P., & Percival, J. W. 2003, ApJS, 149, 405
Hakkila, J., Myers, J. M., Stidham, B. J., & Hartmann, D. H. 1997, AJ, 114, 2043
Hartmann, D., & Burton, W. B. 1997, Atlas of Galactic Neutral Hydrogen (Cambridge; New York: Cambridge University Press)
Hausen, N. R., Reynolds, R. J., Haffner, L. M., & Tufte, S. L. 2002, ApJ, 565, 1060
Heiles, C., Koo, B., Levenson, N. A., & Reach, W. T. 1996a, ApJ, 462, 326
Heiles, C., Reach, W. T., & Koo, B. 1996b, ApJ, 466, 191
Hoopes, C. G., & Walterbos, R. A. M. 2003, ApJ, 586, 902
Hummer, D. G., & Storey, P. J. 1987, MNRAS, 224, 801
Jackson, J. M., Bania, T. M., Simon, R., Kolpak, M., Clemens, D. P., & Heyer, M. 2002, ApJ, 566, L81
Karaali, S., Becker, W., & Fenkart, R. P. 1985, A&AS, 60, 75
Kulkarni, S. R., & Heiles, C. 1987, in ASSL Vol. 134: Interstellar Processes, 87–122
Kutyrev, A. S., Bennett, C. L., Moseley, S. H., Reynolds, R. J., & Roesler, F. L. 2003, in Instrument Design and Performance for Optical/Infrared Ground-based Telescopes. Edited by Iye, Masanori; Moorwood, Alan F. M. Proceedings of the SPIE, Volume 4841, 1201–1210
Lockman, F. J. 2002a, ApJ, 580, L47
Lockman, F. J. 2002b, in ASP Conf. Ser. 276: Seeing Through the Dust: The Detection of HI and the Exploration of the ISM in Galaxies, 107
Lockman, F. J., & Condon, J. J. 2005, AJ, 129, 1968
Lockman, F. J., Jahoda, K., & McCammon, D. 1986, ApJ, 302, 432
Madsen, G. J., Reynolds, R. J., Haffner, L. M., Tufte, S. L., & Maloney, P. R. 2001, ApJ, 560, L135
Mathis, J. S. 1983, ApJ, 267, 119
—. 2000, ApJ, 544, 347
McKee, C. F., & Ostriker, J. P. 1977, ApJ, 218, 148
Meyer, D. M., Cardelli, J. A., & Sofia, U. J. 1997, ApJ, 490, L103+
Mezger, P. O. 1978, A&A, 70, 565
Mierkiewicz, E. 2002, PhD thesis, University of Wisconsin–Madison
Miller, W. W., I., & Cox, D. P. 1993, ApJ, 417, 579
Minter, A. H., Lockman, F. J., Langston, G. I., & Lockman, J. A. 2001, ApJ, 555, 868
Mitra, D., Berkhuijsen, E. M., & Muller, P. 2004, in How does the Galaxy Work?, Granada, in press, ed. E. J. Alfaro, E. Pérez, & J. Franco (Dordrecht: Kluwer)
Nordgren, T. E., Cordes, J. M., & Terzian, Y. 1992, AJ, 104, 1465
Nossal, S., Roesler, F. L., Bishop, J., Reynolds, R. J., Haffner, M., Tufte, S., Percival, J., & Mierkiewicz, E. J. 2001, J. Geophys. Res., 106, 5605
Osterbrock, D. E. 1989, Astrophysics of gaseous nebulae and active galactic nuclei (Mill Valley, CA: University Science Books)
Perryman, M. A. C., Lindegren, L., Kovalevsky, J., Hoeg, E., Bastian, U., Bernacca, P. L., Crézé, M., Donati, F., Grenon, M., van Leeuwen, F., van der Marel, H., Mignard, F., Murray, C. A., Le Poole, R. S., Schrijver, H., Turon, C., Arenou, F., Froeschlé, M., & Petersen, C. S. 1997, A&A, 323, L49
Popowski, P. 2000, ApJ, 528, L9
Rand, R. J. 1997, ApJ, 474, 129
Reichen, M., Lanz, T., Golay, M., & Huguenin, D. 1990, Ap&SS, 163, 275
Reynolds, R. J. 1990, ApJ, 349, L17
Reynolds, R. J. 1991a, in IAU Symp. 144: The Interstellar Disk-Halo Connection in Galaxies, 67–76
—. 1991b, ApJ, 372, L17
Reynolds, R. J., Haffner, L. M., & Tufte, S. L. 1999, ApJ, 525, L21
Roshi, D. A., & Anantharamaiah, K. R. 2001, ApJ, 557, 226
Ruffle, P. M. E., Zijlstra, A. A., Walsh, J. R., Gray, M. D., Gesicki, K., Minniti, D., & Comeron, F. 2004, MNRAS, 353, 796
Scherb, F. 1981, ApJ, 243, 644
Schlegel, D. J., Finkbeiner, D. P., & Davis, M. 1998, ApJ, 500, 525
Sembach, K. R., Howk, J. C., Ryans, R. S. I., & Keenan, F. P. 2000, ApJ, 528, 310
Shaver, P. A. 1980, A&A, 91, 279
Simpson, J. P., Rubin, R. H., Colgan, S. W. J., Erickson, E. F., & Haas, M. R. 2004, ApJ, 611, 338
Spitzer, L. J., & Fitzpatrick, E. L. 1993, ApJ, 409, 299
Stanek, K. Z. 1996, ApJ, 460, L37
Straižys, V., Černis, K., & Bartašiūtė, S. 2003, A&A, 405, 585
Taylor, J. H., & Cordes, J. M. 1993, ApJ, 411, 674
Tufte, S. L. 1997, PhD thesis, University of Wisconsin–Madison
Tufte, S. L., Reynolds, R. J., & Haffner, L. M. 1998, ApJ, 504, 773
Udalski, A. 2003, ApJ, 590, 284
Walton, N. A., Barlow, M. J., & Clegg, R. E. S. 1993, in IAU Symp. 153: Galactic Bulges, 337
Weymann, R. J., Vogel, S. N., Veilleux, S., & Epps, H. W. 2001, ApJ, 561, 559
Wilson, C. D. 1995, ApJ, 448, L97
York, D. G., & Rogerson, J. B. 1976, ApJ, 203, 378

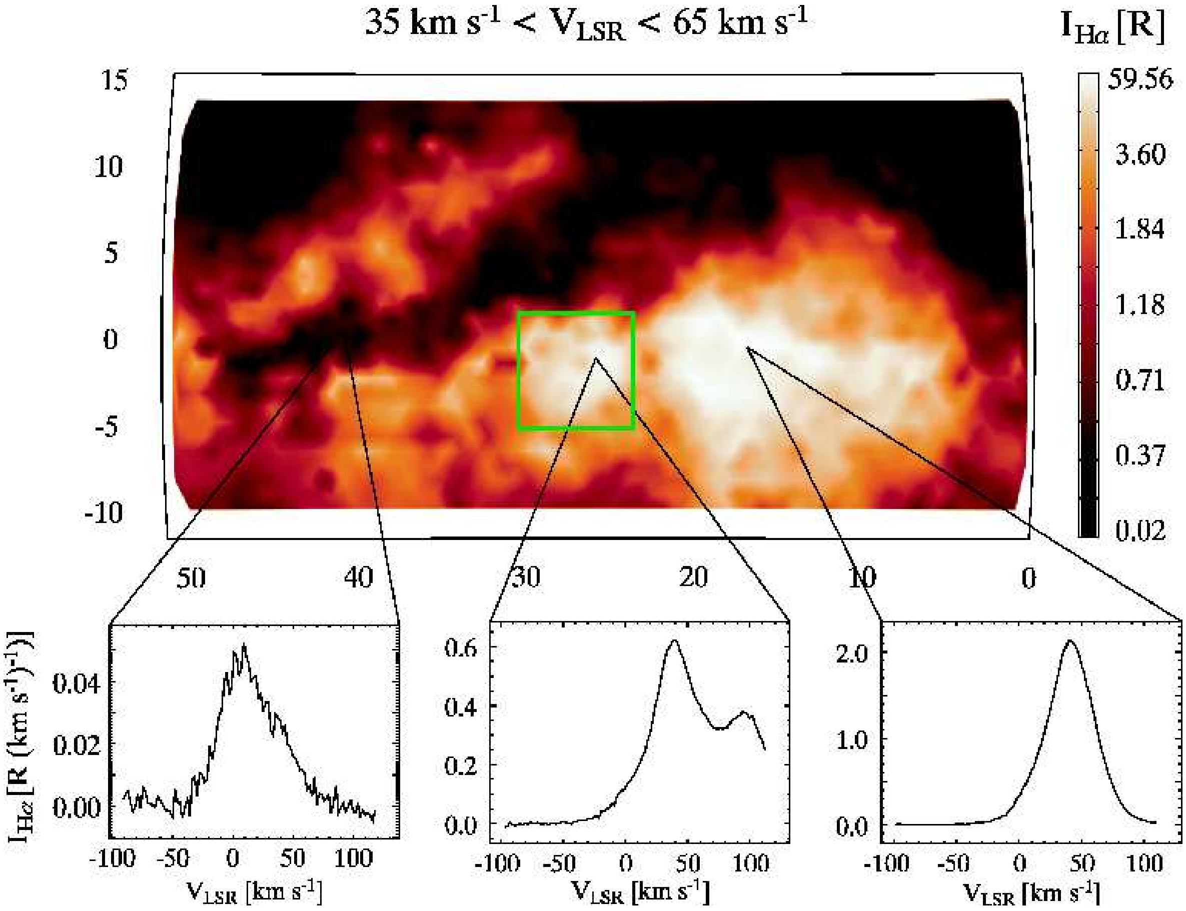

FIG. 1.— Hα map and spectra from the WHAM-NSS toward the inner Galaxy. The large dark feature in the middle of the map is the Aquila rift, a nearby dust cloud (d ≈ 250 pc) that is obscuring the Hα emission behind it with $v_{\rm LSR} > +25$ km s^{-1}. The three diagrams below the map show the Hα spectra toward the indicated directions, revealing the change in the obscuration of emission from the local neighborhood (0 km s^{-1}), the Sagittarius arm (+50 km s^{-1}), and the Scutum arm (+80 km s^{-1}). Note the significant change in the intensity scale between these spectra. The green box is the low extinction window toward the 'Scutum Star Cloud' with emission out to the tangent point velocity.

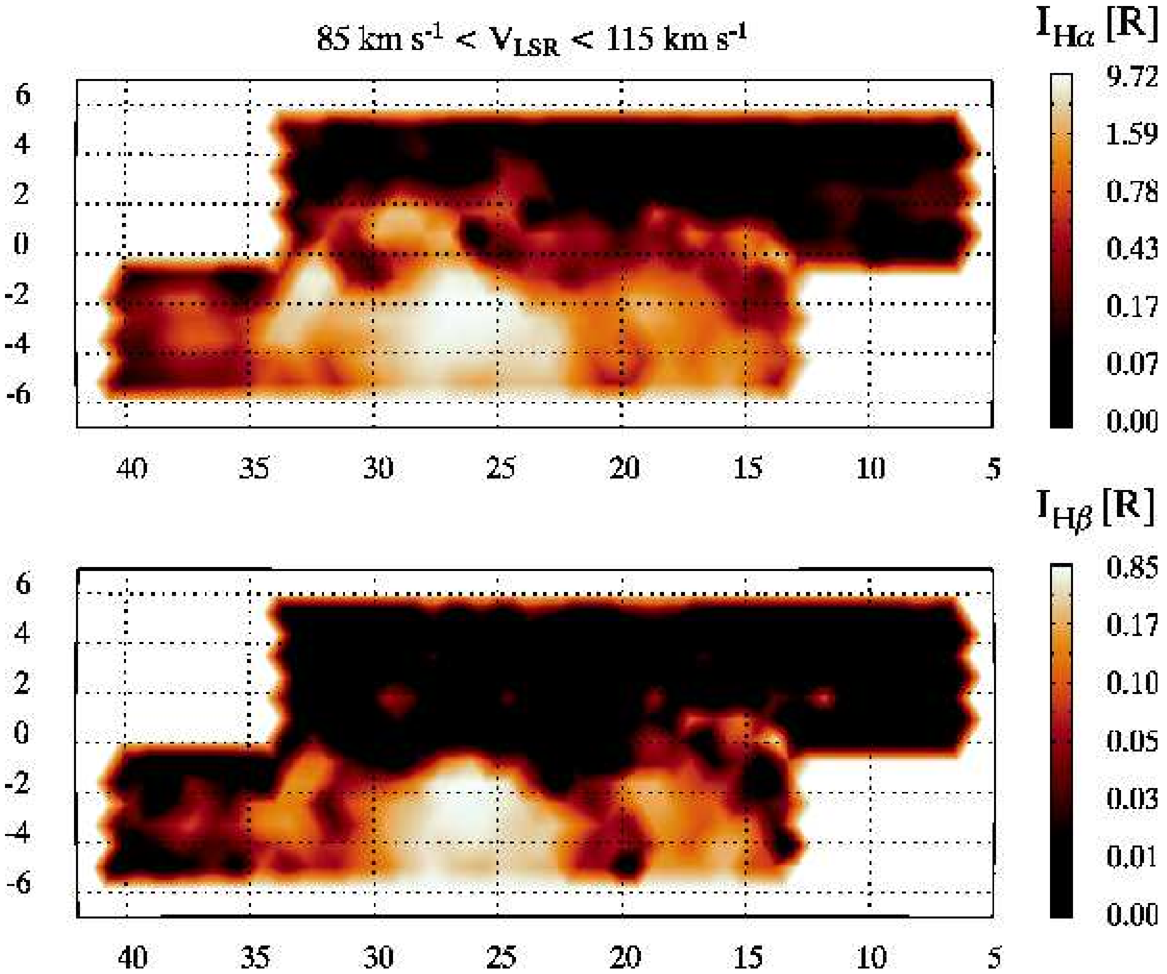

FIG. 2.— Histogram equalized map of Hα and Hβ emission toward the inner Galaxy at high velocity, with $+85 \ \mathrm{km\,s^{-1}} < v_{\mathrm{LSR}} < +115 \ \mathrm{km\,s^{-1}}$. The spectra near $(\ell, b) = (27°, -3°)$ have an emission line centered near $v_{\mathrm{LSR}} \approx +100 \ \mathrm{km\,s^{-1}}$, suggesting that we are seeing emission out to the tangent point at a heliocentric distance $D_\odot \gtrsim 6$ kpc.

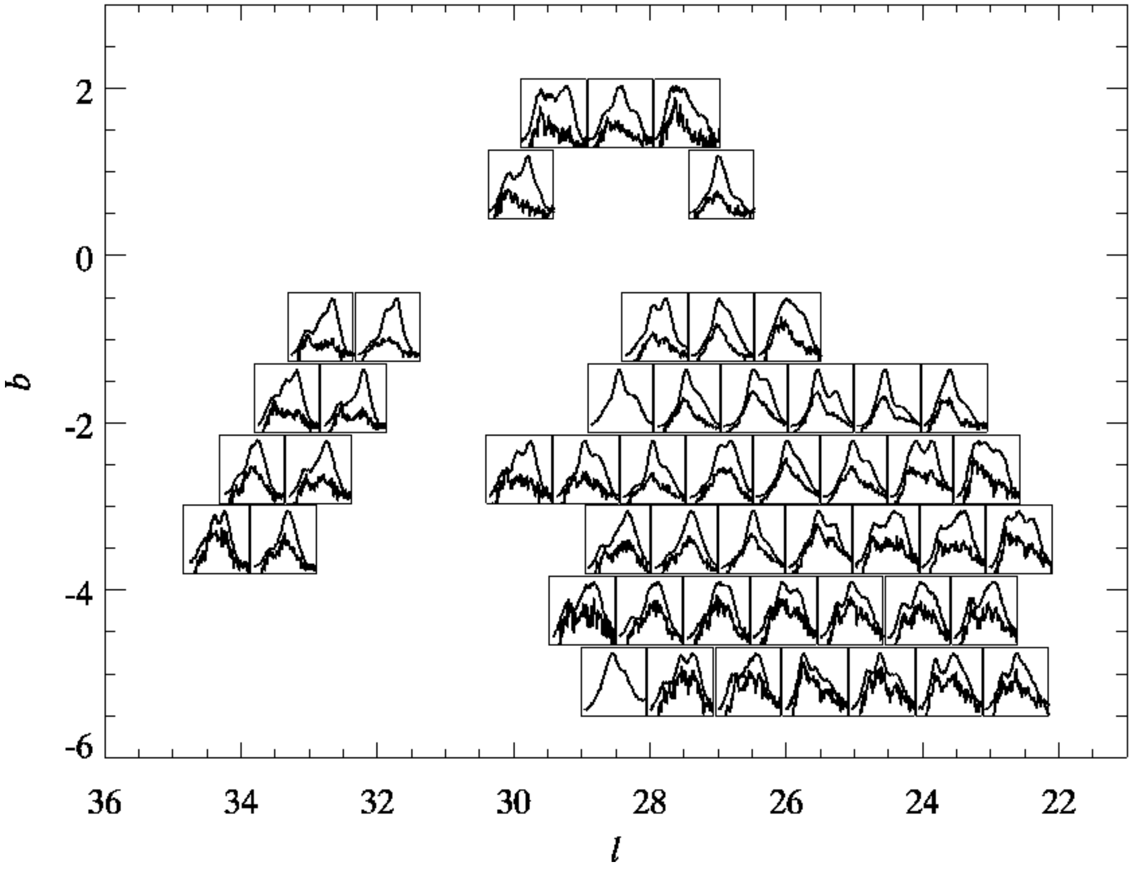

FIG. 3.— Combination of spectral and spatial information for 51 directions which show Hα emission at $v_{\rm LSR} \gtrsim +100$ km s^{-1}. Each square shows a full Hα and Hβ spectrum and location of that spectrum on the sky. The emission is shown over a fixed velocity range, -50 km s^{-1} to +150 km s^{-1} in each spectrum, with an arbitrary vertical scale. The Hβ spectra have been multiplied by 3.94, the expected ratio of Hα/Hβ in the absence of extinction. Note the increase in Hβ/Hα, or decrease in $A(V)$, with increasing angular distance away from the Galactic plane and at lower $v_{\rm LSR}$. For two directions no reliable Hβ spectra were obtained.

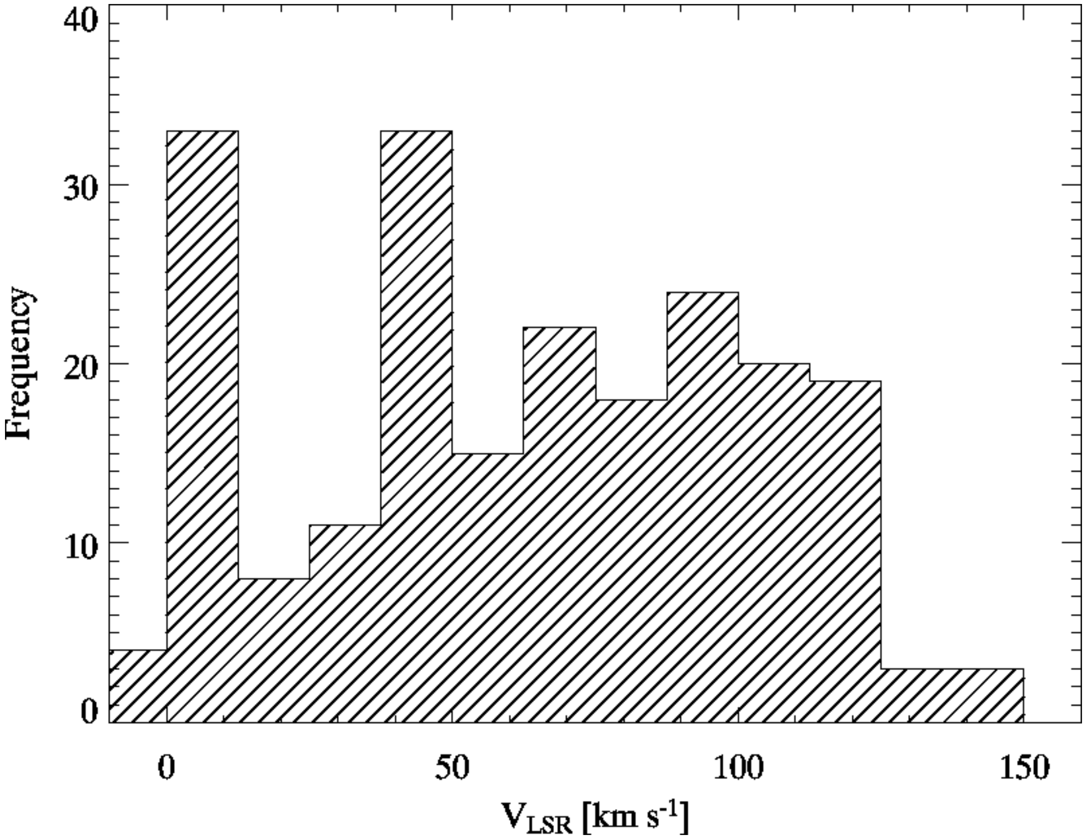

Fig. 4.— Histogram of the component velocities for the Hα spectra in the low-extinction window shown in Figure 3. The velocities were determined through a least-squares fit of Gaussian profiles to the spectra. The width of each bin is 12.5 $\mathrm{km\,s^{-1}}$. There are two peaks near 0 $\mathrm{km\,s^{-1}}$ and +50 $\mathrm{km\,s^{-1}}$, corresponding to emission from the solar neighborhood and the Sagittarius spiral arm, respectively.

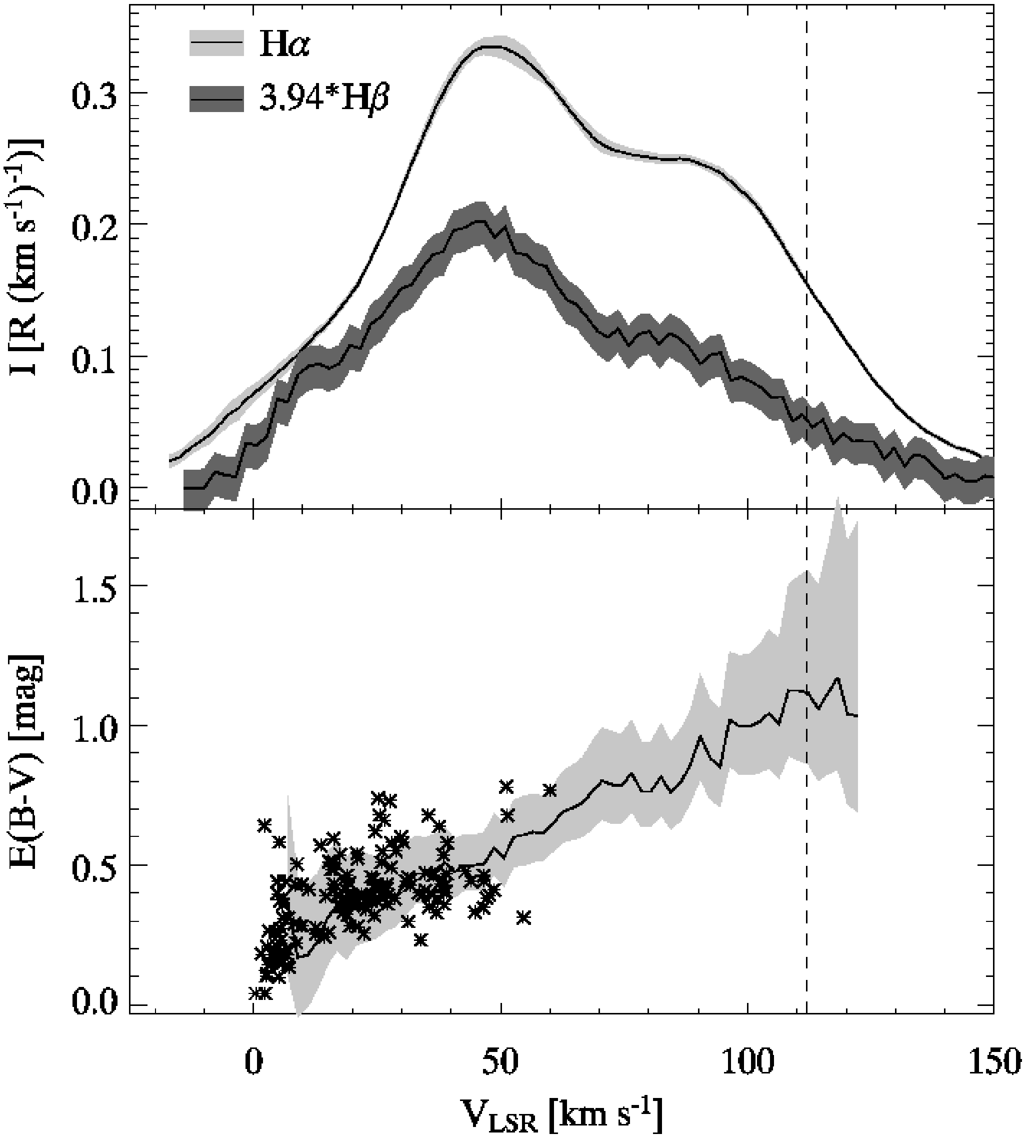

FIG. 5.— Comparison of extinction measurements with those of Reichen et al. (1990) toward the Scutum cloud. The top panel shows the average of nine Hα and Hβ spectra within the low $E(B-V)$ area outlined by (Reichen et al. 1990), with the shaded regions representing the systematic uncertainties. The bottom panel shows the inferred value of $E(B-V)$ from the Hα and Hβ spectra. The asterisks are measured values of $E(B-V)$ for several UV bright stars in this area, where the distance to each star was converted to an LSR velocity using the rotation curve of Clemens (1985). The dashed vertical line is the location of the tangent point velocity. We find that the two data sets agree within the uncertainties.

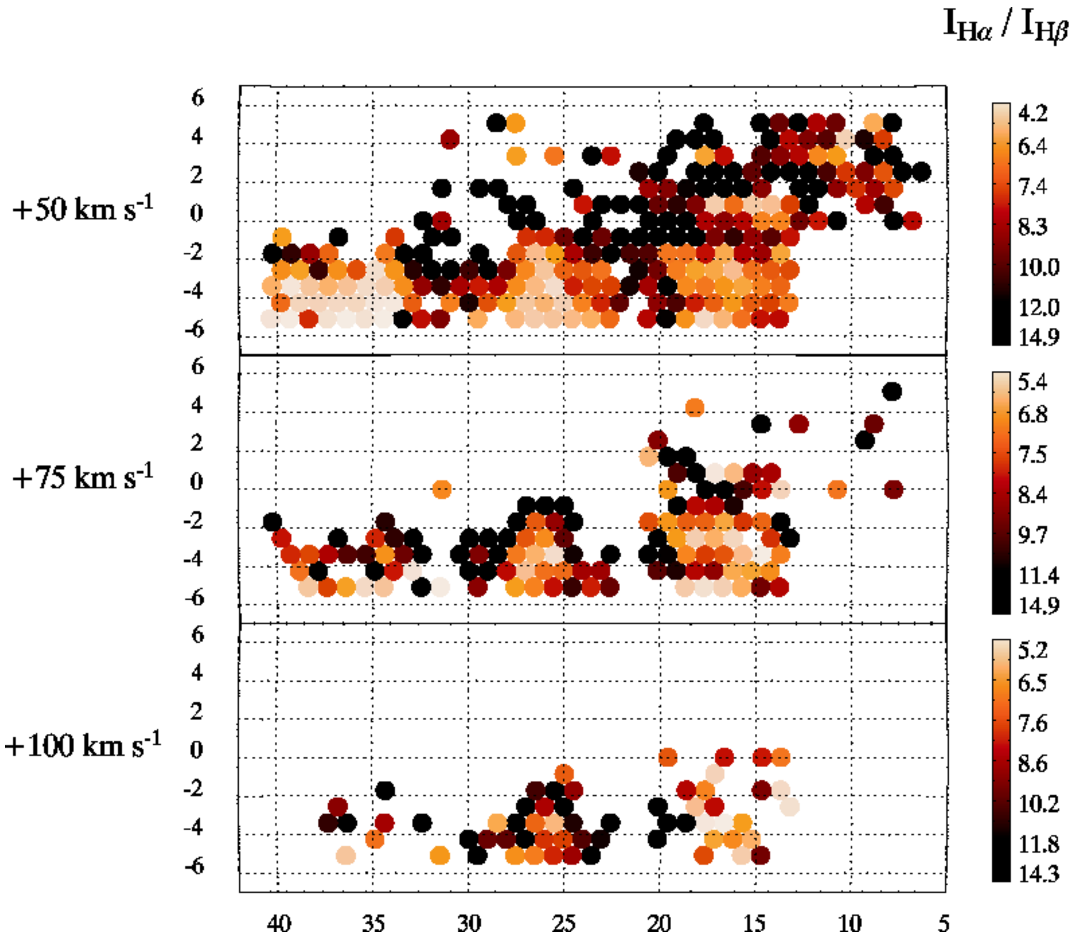

FIG. 6.— Three velocity channel maps of the average ratio of $I_{\mathrm{H}\alpha}/I_{\mathrm{H}\beta}$ at $v_{\mathrm{LSR}} = +50$ km s^{-1}, $+75$ km s^{-1}, and $+100$ km s^{-1}, over a width of 25 km s^{-1}. Observations with large uncertainties have been omitted. Note the area of low $I_{\mathrm{H}\alpha}/I_{\mathrm{H}\beta}$ near (27°, -3°), in which the extinction remains low out to near the tangent point velocity.

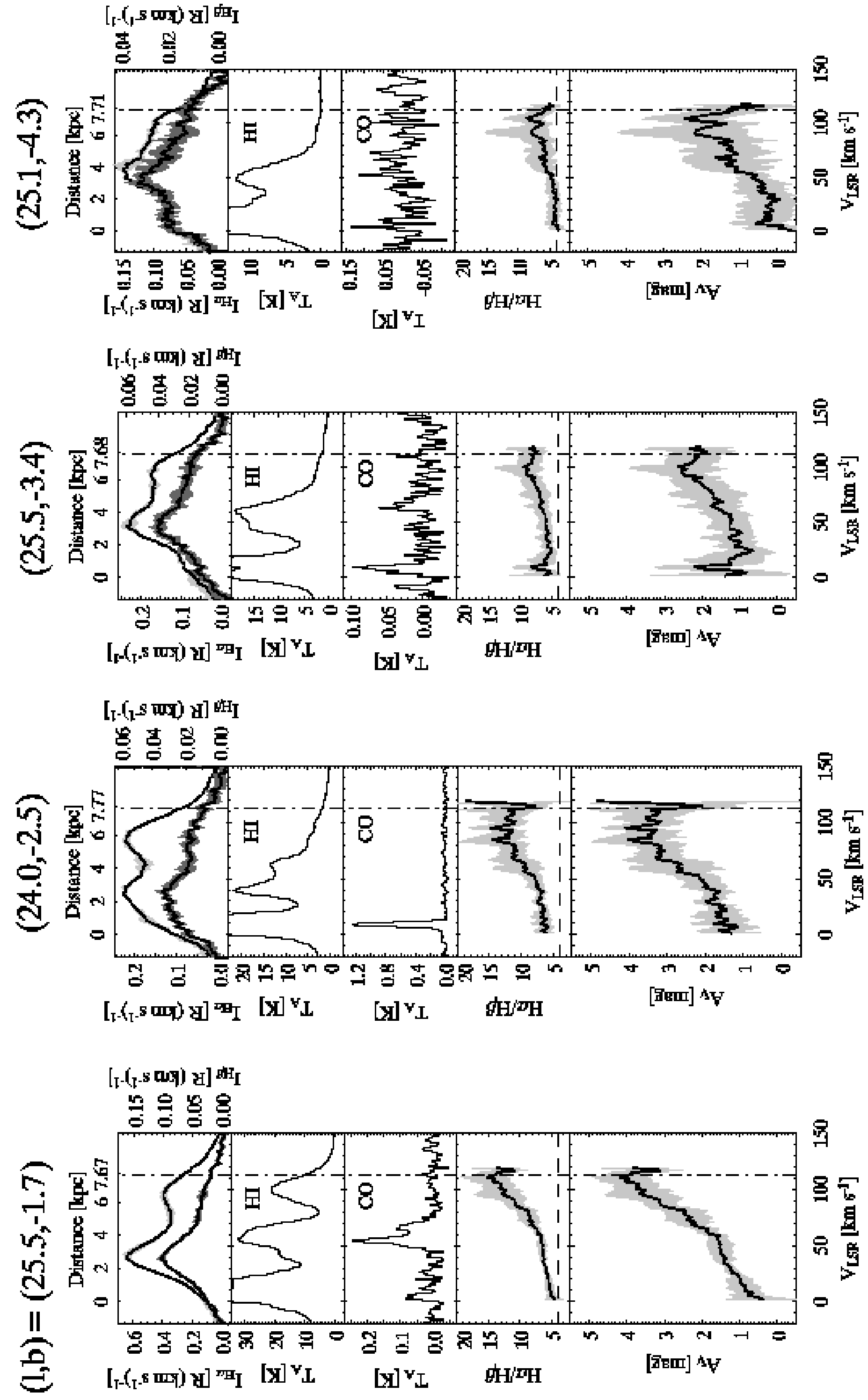

FIG. 7.— Sample of spectra for four sightlines in this study, along with other tracers of the ISM. Notice the increase in $A(V)$ with increasing distance/velocity, and the relationship between the shape of the $A(V)$ curve and the H I and CO spectra (see §4.4).

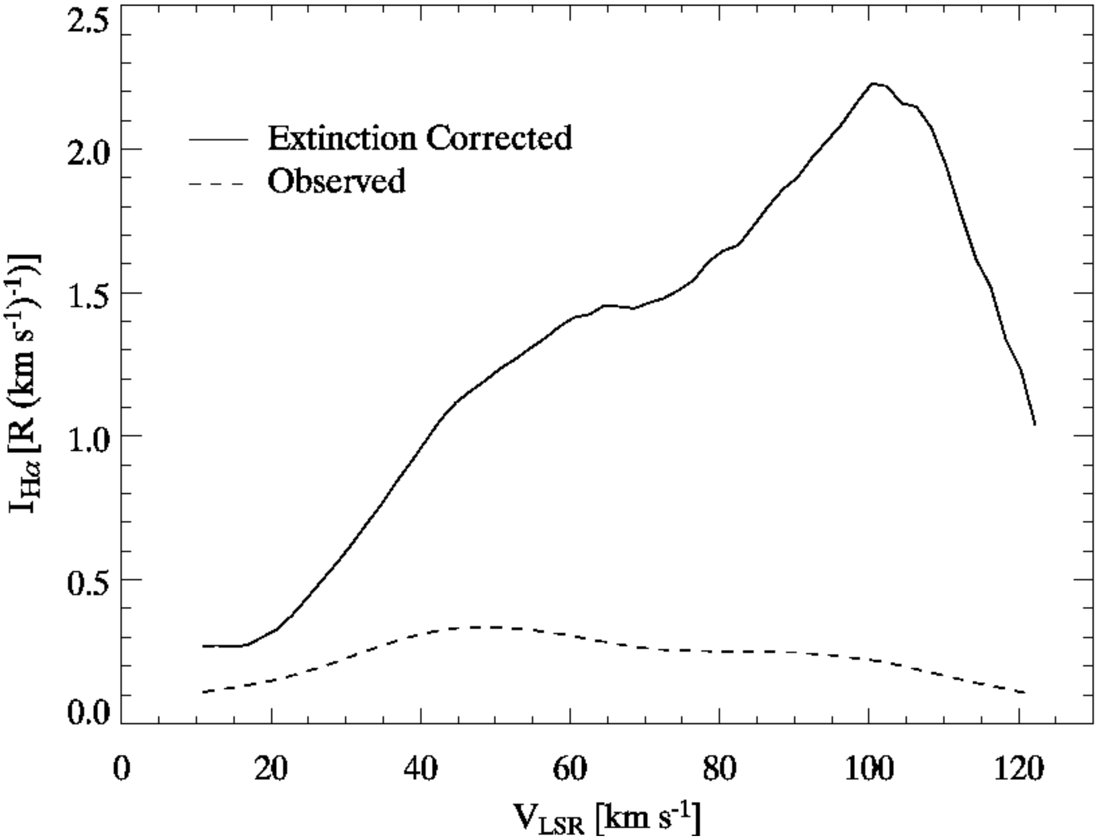

FIG. 8.— Comparison of the observed and extinction corrected Hα emission toward the window. The observed spectrum is the average of the same nine spectra used in Figure 5. The optical depth at each velocity data point was inferred from the average ratio of $I_{\mathrm{H}\alpha}/I_{\mathrm{H}\beta}$ in a 25 km s^{-1} window around each data point (see §4.4). Note the particularly strong emission at $v_{\mathrm{LSR}} \approx +105$ km s^{-1}, which is near the tangent point velocity.

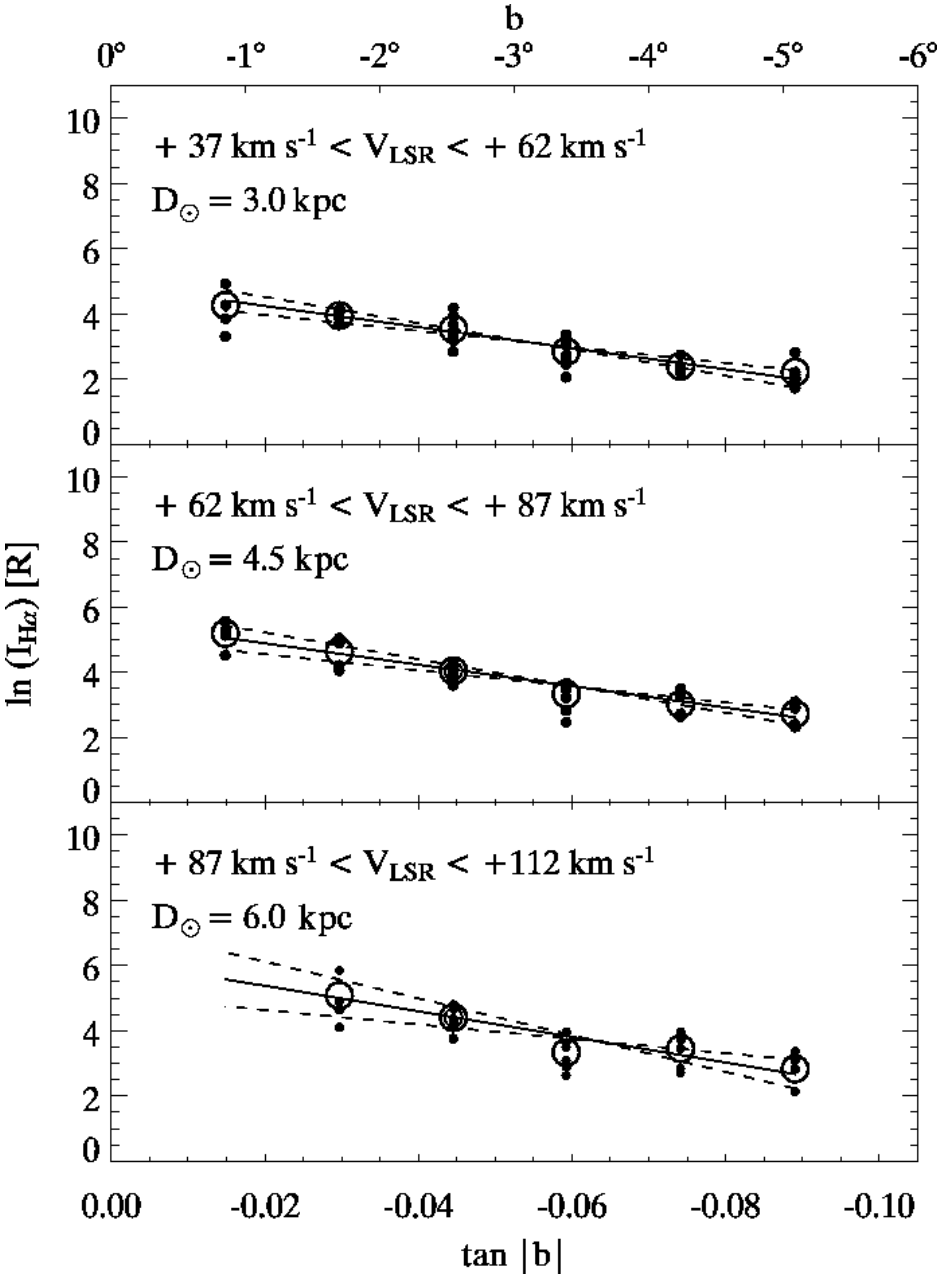

Fig. 9.— Extinction-corrected Hα emission vs. angular distance from the Galactic plane for emission at three different radial velocity intervals. The assumed heliocentric distances $D_\odot$ to the emission regions are also shown. A best fit line to the data and the uncertainty is shown as solid and dashed lines, respectively (see §5).

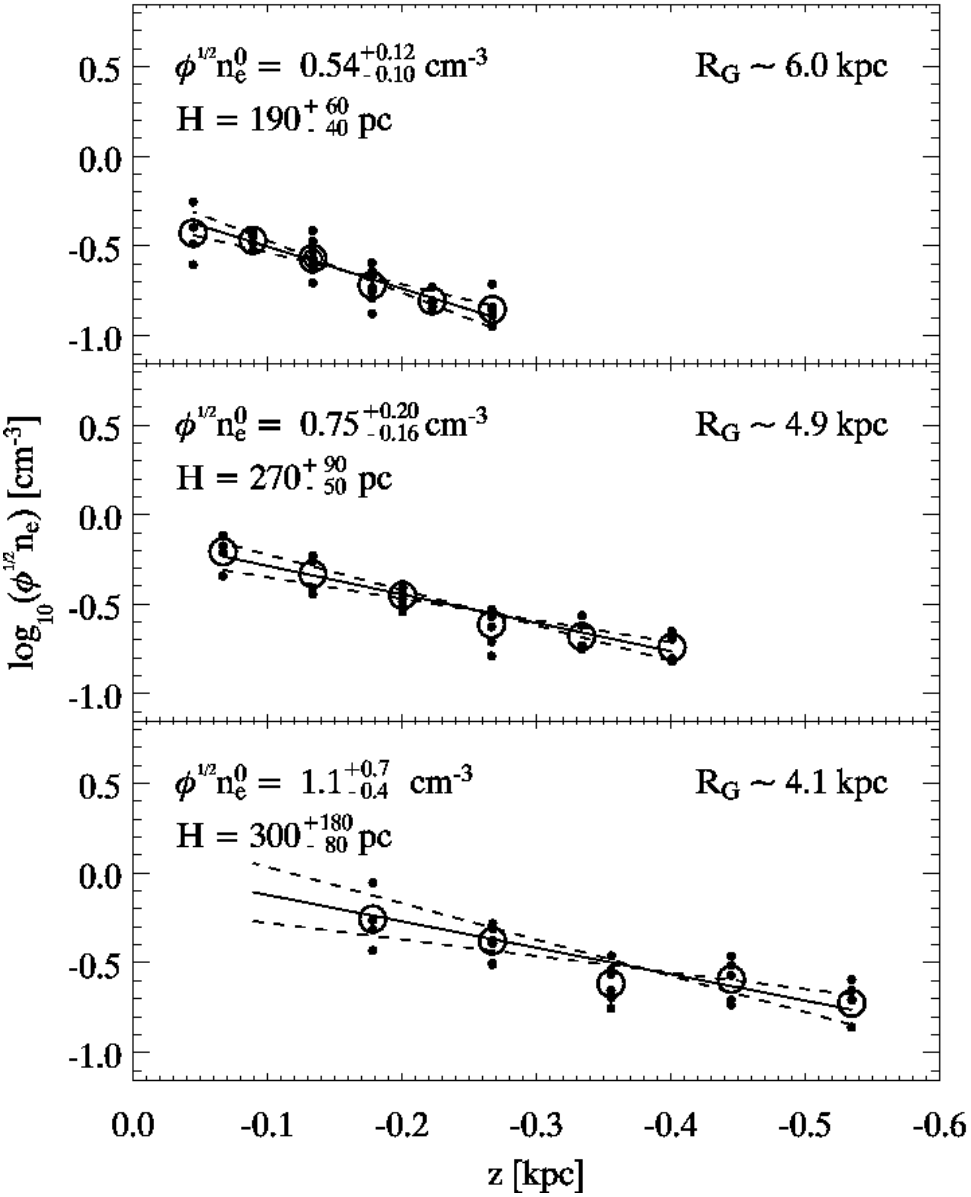

FIG. 10.— Same as Figure 9, except the observable quantities of $I_{\mathrm{H}\alpha}$ and b have been converted into the physical quantities of density n_e and vertical height z, as described in §5. The best-fit values for the rms midplane density $\phi^{1/2}n_e^0$ and scale height H are shown in the upper left. The assumed distance from the center of the Galaxy to the gas described by these physical parameters is also shown.

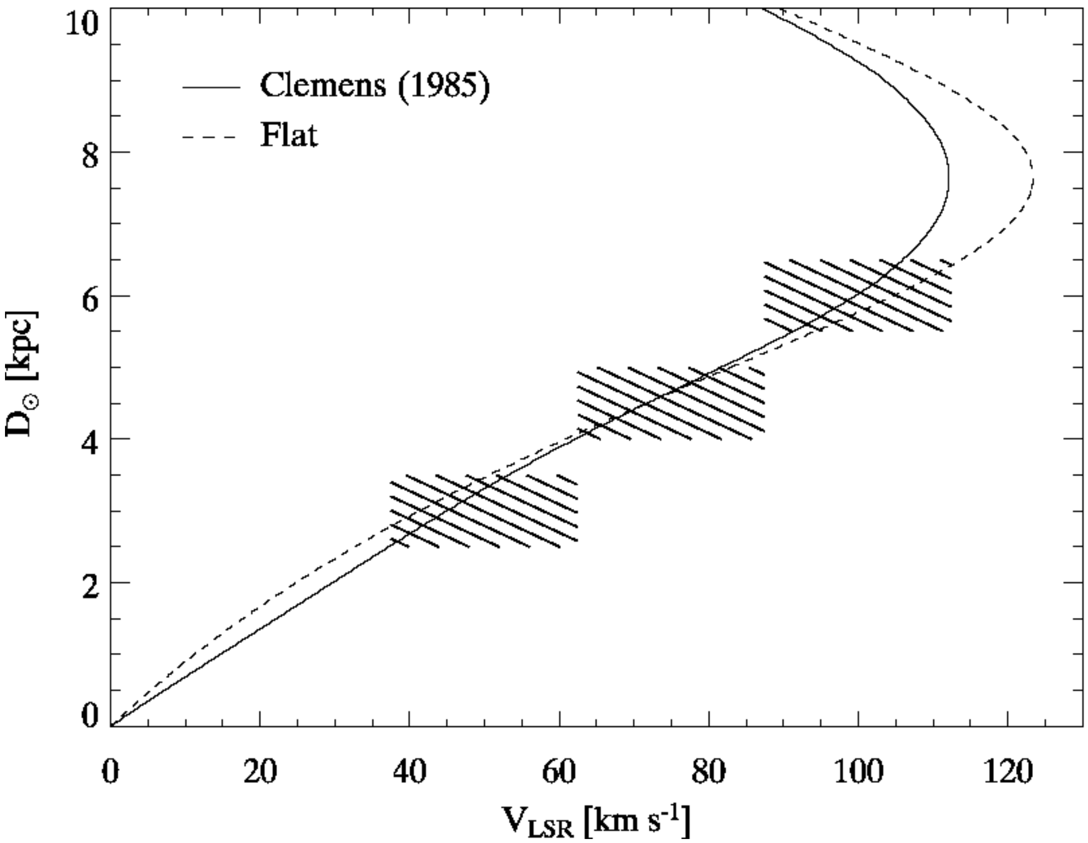

FIG. 11.— Relationship between LSR velocity and heliocentric distance toward $(\ell, b) = (26.5°, -2.5°)$ for two different rotation curves. The rotation curve from Clemens (1985) and a flat curve, assuming $\Omega = 220$ km s^{-1} and $R_\odot = 8.5$ kpc, are represented by the solid and dashed lines, respectively. The three hatched regions show the extent of our assumed distances to the Hα emission over three different velocity intervals, as discussed in §5.

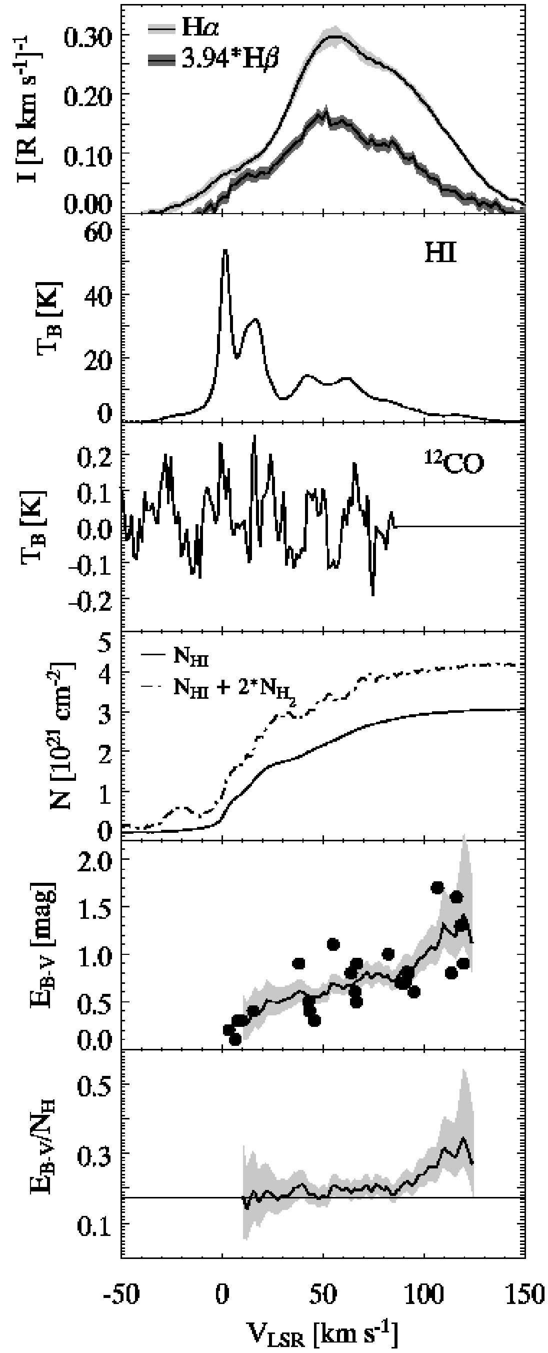

FIG. 12.— Comparison of $E(B-V)/N_{\rm H}$ toward the low extinction window from our data with the canonical value from Bohlin et al. (1978). The H I and CO data are from Hartmann & Burton (1997) and Dame et al. (2001), respectively. The bottom panel, with $E(B-V)/N_{\rm H}$ given in units of mag per 10^{21} cm^{-2}, shows good agreement between our data (*shaded*) and the Bohlin et al. (1978) value (*straight line*), with evidence for a larger extinction per unit hydrogen atom in the inner Galaxy (see §7).

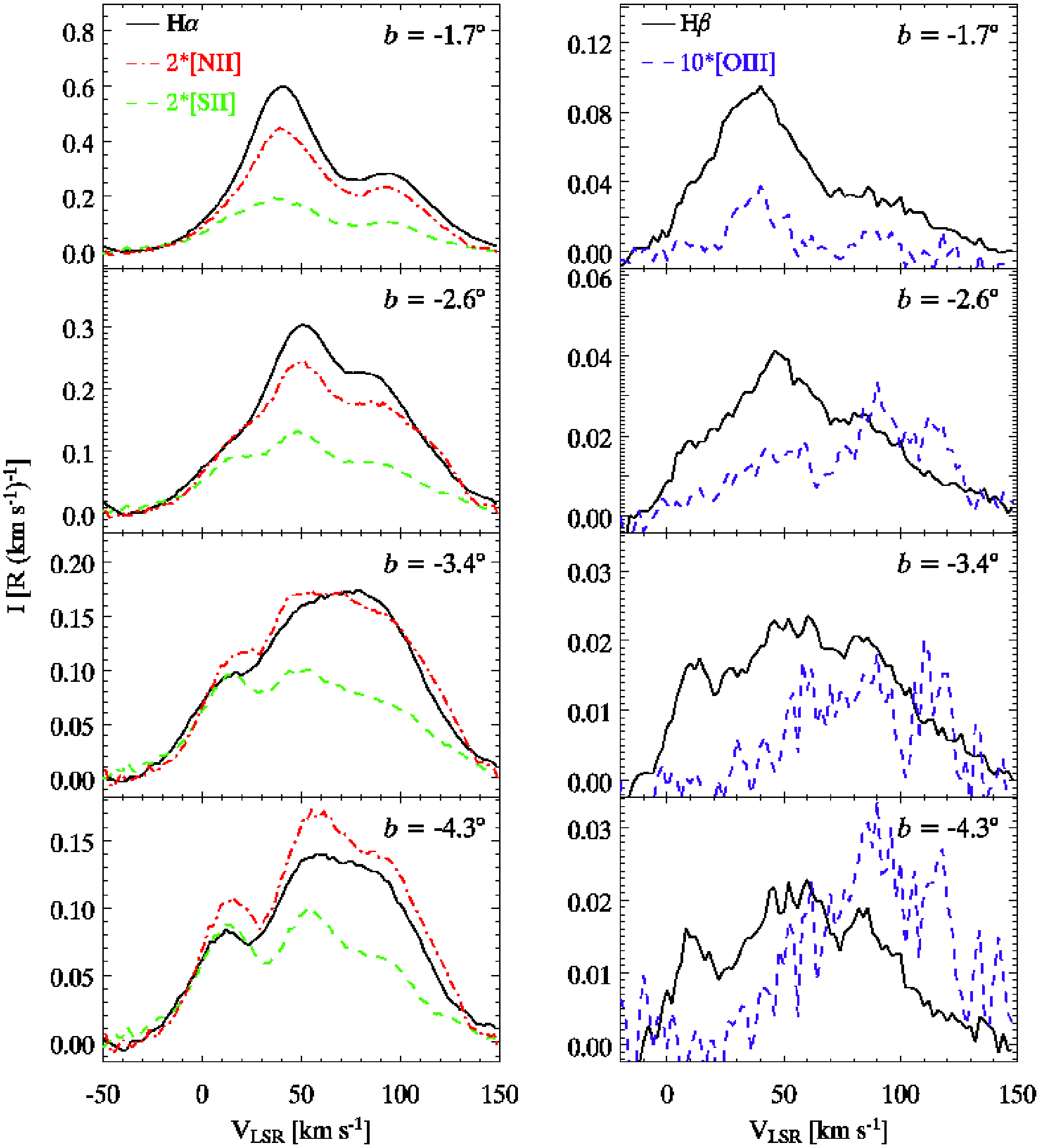

FIG. 13.— Emission line spectra toward the window. Thirteen sightlines were observed in emission lines that probe the temperature and ionization state of the gas. The left panel shows the average Hα (*black*), [N II] (*red*), and [S II] (*green*) spectra at each latitude. The right panel is the same, but for Hβ (*black*) and [O III] (*purple*). Some of the spectra have been multiplied by the indicated values to facilitate a visual comparison of the profiles. Note the increase in [N II]/Hα and [S II]/Hα with increasing distance from the plane. Also note the large increase in [O III]/Hβ with distance from the plane at high velocities (i.e., in the inner Galaxy).

TABLE 1
Summary of [N II], [S II], and [O III] Observations

v_{LSR}[a]		b			
		-1.7°	-2.6°	-3.4°	-4.3°
+25 km s^{-1}	$I_{\mathrm{H}\alpha}$ [R]	22.8	11.9	8.8	6.4
	[N II]/Hα	0.39	0.48	0.58	0.61
	[S II]/Hα	0.19	0.28	0.38	0.42
	[S II]/[N II]	0.47	0.58	0.66	0.69
	[O III]/Hα	0.006	0.007	0.002	0.002
+50 km s^{-1}	$I_{\mathrm{H}\alpha}$ [R]	44.7	34.2	15.1	9.8
	[N II]/Hα	0.37	0.40	0.54	0.61
	[S II]/Hα	0.15	0.20	0.29	0.33
	[S II]/[N II]	0.41	0.50	0.54	0.54
	[O III]/Hα	0.010	0.013	0.018	0.042
+75 km s^{-1}	$I_{\mathrm{H}\alpha}$ [R]	30.9	23.6	25.2	19.8
	[N II]/Hα	0.41	0.39	0.48	0.56
	[S II]/Hα	0.17	0.17	0.22	0.25
	[S II]/[N II]	0.42	0.44	0.45	0.45
	[O III]/Hα	<0.000	0.010	0.018	0.024
+100 km s^{-1}	$I_{\mathrm{H}\alpha}$ [R]	56.3	44.6	27.4	19.8
	[N II]/Hα	0.40	0.44	0.49	0.57
	[S II]/Hα	0.17	0.18	0.22	0.23
	[S II]/[N II]	0.42	0.40	0.43	0.40
	[O III]/Hα	0.002	0.018	0.037	0.065

[a] Emission is averaged over longitude, and integrated over a 25 km s^{-1} interval centered at the given velocity. All of the data have been corrected for extinction, and the line ratios are given in energy units.